Table 1
List of proteins differentially expressed between *gad* and WT mice.

Spot no.	Protein name	Score	Molecular mass (kDa)/pI	Av. ratio (*gad*/wt) 12 weeks	*P* value	Av. ratio (*gad*/wt) 2 weeks	*P* value
1	Ubiquitin thiolesterase PGP9.5 (UCH-L1)	96	25.10/5.12	−14.38	0.005	−3.89	0.003
3	14-3-3 protein	94	28.10/4.63	5.4	0.030	7.32	0.001
4	Annexin A5	143	35.79/4.83	6.68	0.020	5.19	0.030
8	Neurofilament triplet L protein (NF-L)	212	61.40/4.62	2.18	0.010	3.53	0.026
5	Glyceraldehyde 3-phosphate dehydrogenase (GAPDH)		38.07/8.34	3.89	0.043	1.61	

*GAPDH was detected by 2D Western blotting and not by MALDI-TOF/TOF.

Fig. 1A shows a representative pseudocolor picture of superimposed DIGE images of the 12-week-old mouse samples. Fourteen protein spots were increased by at least 1.6-fold in *gad* mice compared with WT mice (red; Student's paired *t*-test value; $P < 0.05$ in 3 parallel gels), and one spot was not detected at all in *gad* mice (green).

Fig. 1B shows a representative pseudocolor picture of superimposed DIGE images of the 2-week-old mouse samples. Eighteen protein spots were increased by at least 1.6-fold in *gad* mice compared with WT mice (red; Student's paired *t*-test value; $P < 0.05$ in 3 parallel gels), and one spot was not detected at all in *gad* mice (green).

Based on comparison of the 2D-DIGE analysis of mice between 2 and 12 weeks old, 7 protein spots showed an age-dependent increase in *gad* mice (spots No. 2–8). One spot (spot No. 1) was not detected at all in *gad* mice at either 2 or 12 weeks old (Fig. 1A and B).

Fig. 1C shows the 3D images of typical spots (spots No. 1, 3, and 5) in Fig. 1A, and Fig. 1D shows the 3D images of typical spots (spots No. 1, 3, and 5) in Fig. 1B.

3.2. Identification of differentially expressed proteins between gad and WT mice by MALDI-TOF/TOF and 2D Western blotting

The proteins of spots that were age dependently increased or absent in *gad* mice were analyzed by MALDI-TOF/TOF and identified (spots No. 1, 3, 4, and 8). The proteins were identified as UCH-L1 (spot No. 1), 14-3-3 (spot No. 3), annexin V (spot No. 4), and Neurofilament L (NF-L) (spot No. 8). Additionally, we speculated that spot No. 5 may represent GAPDH based on the information from the mouse brain proteome database (http://www.charite.de/humangenetik/klose_public1/index.html), and confirmed this by 2D Western blotting with GAPDH antibodies. The results of the protein identification are listed in Table 1, including spot number, protein name, mascot score, theoretical relative molecular mass, isoelectric point, average ratio of *gad*/wt protein level, and *P*-value using DeCyder, at both 2 and 12 weeks old.

3.3. Analyses of the expression levels of proteins in gad and WT mice by Western blotting

In 2D-DIGE system, each sample was pre-labeled with different fluorescence dyes, Cy3, Cy5 or Cy2. This labeling-process allows comparison of multiple samples in same 2D-gel, but it is reported that efficiency of each dyes to label proteins was not exactly the same. We assume that 2D-DIGE is reliable method to detect molecules involved in axonal degeneration but Western blot analysis using specific antibodies is more accurate, and in fact, it is usual that identified proteins by TOF-MASS are reconfirmed by Western blotting. Therefore, the expression levels of the proteins in

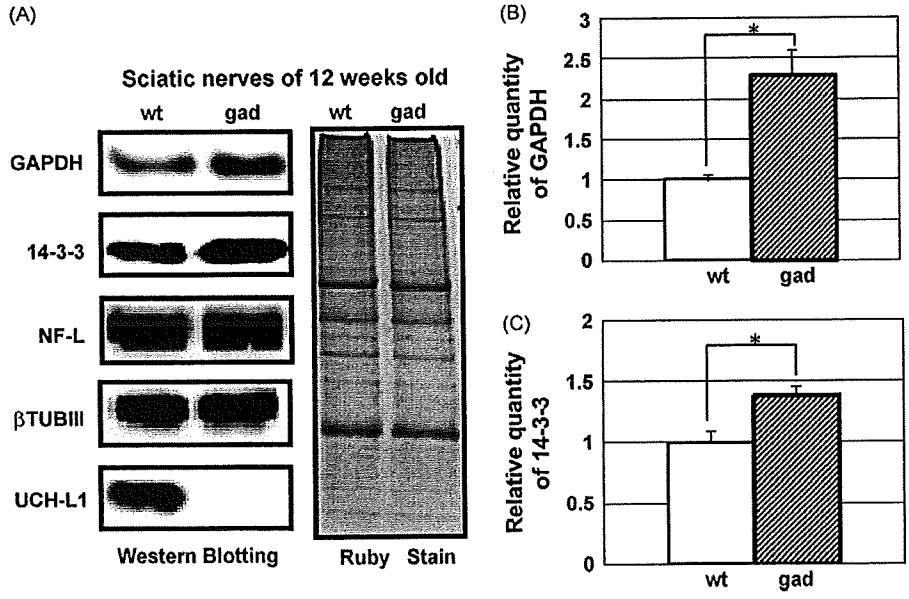

Fig. 2. Western blotting analyses of the expression levels of proteins expressed differentially between *gad* and WT mice.
(A) Results of Western blotting analysis with antibodies against ubiquitin carboxyl-terminal hydrolase L1 (UCH-L1), neurofilament L (NF-L), 14-3-3, glyceraldehyde-3-phosphate dehydrogenase (GAPDH), and classIII β tubulin (βTUBIII). GAPDH and 14-3-3 protein levels were increased in *gad* mice compared with WT mice.
(B) Quantification of the band intensities of GAPDH. Values are means ± SEM of 3 independent experiments (*$P < 0.05$); GAPDH is increased by about 2.3-fold in *gad* mice at 12 weeks old compared with WT mice.
(C) Quantification of the band intensities of 14-3-3. Values are means ± SEM of 3 independent experiments (*$P < 0.05$); 14-3-3 is increased by 1.3-fold in *gad* mice at 12 weeks old compared with WT mice.

gad and WT mice listed in Table 1 were further analyzed by Western blotting to reconfirm the results of 2D-DIGE (Fig. 2A). We chose these proteins because they were all reported to be expressed in neurons. In 12-week-old *gad* mice, GAPDH was increased by an average ratio of 2.3-fold (Fig. 2B), and 14-3-3 was increased by an average ratio of 1.3-fold (Fig. 2C) compared with WT mice. The levels of NF-L and βTUBIII, which was used as an internal control, showed no significant difference between *gad* and WT mice at 12 weeks old (Fig. 2A). Annexin V was not analyzed because its antibodies did not work in this experimental system containing urea and thiourea. The same results were obtained in 3 independent experiments.

3.4. Histochemical localization of GAPDH in the sciatic nerves of gad and WT mice

Sciatic nerves are composed internally of neuronal axons and externally of myelin derived from glial Schwann cells, and protein samples in the proteomic analysis were a mixture of axons and myelin. We examined the histological localization of GAPDH, which was dominantly increased in *gad* mice, by double immunofluorescence staining using an antibody against GAPDH and the neuronal markers neurofilament M (NF-M) or UCH-L1, or the Schwann cells marker myelin basic protein (MBP). In *gad* mice, GAPDH was colocalized with MBP (Fig. 3A, right panel) but was more dominantly colocalized with NF-M, a neuronal marker (Fig. 3A, left panel). These results suggest that GAPDH is mainly localized in axons in *gad* mice. In WT mice, GAPDH was colocalized with the neuronal marker UCH-L1 (Fig. 3B, left panel). Because UCH-L1 is the product of the gene defective in the *gad* mouse, UCH-L1 is not detected in *gad* mice (Fig. 3B, right panel). The same results were obtained in 3 independent experiments.

3.5. DAB staining analyses of GAPDH and 14-3-3 in the sciatic nerves of gad and WT mice

We examined in detail the localization of GAPDH in cross or vertical sections of sciatic nerve axons by DAB staining (Figs. 4A–F). In the cross-sections, GAPDH was localized in axons in both *gad* and WT mice and was remarkably accumulated in *gad* mice compared with WT mice (Fig. 4A and B). In vertical sections, GAPDH was also localized in axons in both *gad* and WT mice (Fig. 4C–F). Notably, aggregates of GAPDH were observed in *gad* mice but not in WT mice (Fig. 4E and F, arrow). Next, we examined the expression of 14-3-3, which was found to be increased in *gad* mice upon 2D-DIGE and Western blotting analyses. In both *gad* and WT mice, 14-3-3 was expressed in axons, and there was no significant difference between *gad* and WT mice (Fig. 4G–J). The same results were obtained in 3 independent experiments.

3.6. Histochemical analyses of sulfonated GAPDH in the sciatic nerves of gad and WT mice

It was reported that oxidative stress induces the oligomerization and aggregation of GAPDH (Cumming and Schubert, 2005; Nakajima et al., 2007), and in this study we found that GAPDH is accumulated in axons of *gad* mice that exhibit a dying-back-type of axonal degeneration. Thus, we postulated that oxidative stress would be increased in *gad* mice, and therefore examined the expression of sulfonated GAPDH (Hara et al., 2005), in the sciatic

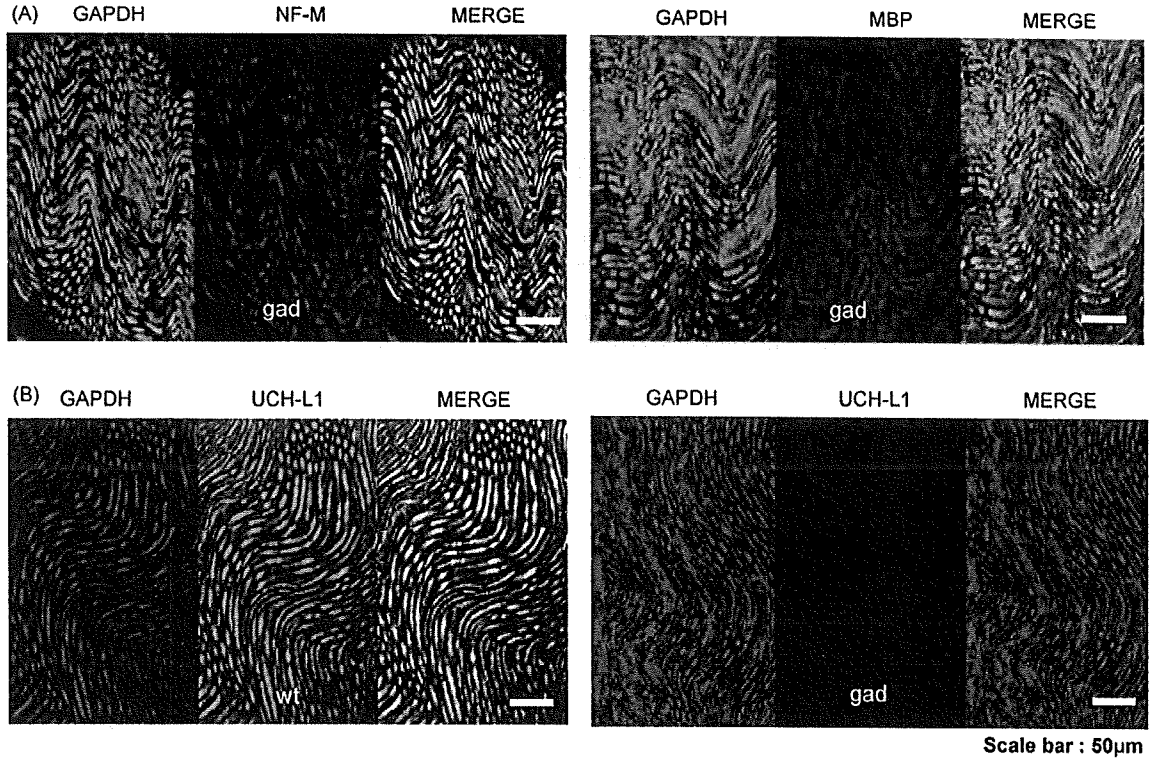

Fig. 3. Histochemical localization of GAPDH in the sciatic nerves of *gad* and WT mice.
(A) Double immunofluorescent staining of the sciatic nerve of *gad* mice using antibodies against GAPDH, neurofilament M (NF-M), or myelin basic protein (MBP). GAPDH was colocalized with NF-M (left panel) and partly with MBP (right panel) in *gad* mice. GAPDH is mainly localized in axons.
(B) Double immunofluorescent staining of the sciatic nerve of *gad* and WT mice using antibodies against GAPDH and UCH-L1. In WT mice, GAPDH is colocalized with UCH-L1 (left panel). In *gad* mice, UCH-L1 is not detected (right panel), and GAPDH is strongly detected compared with WT mice.

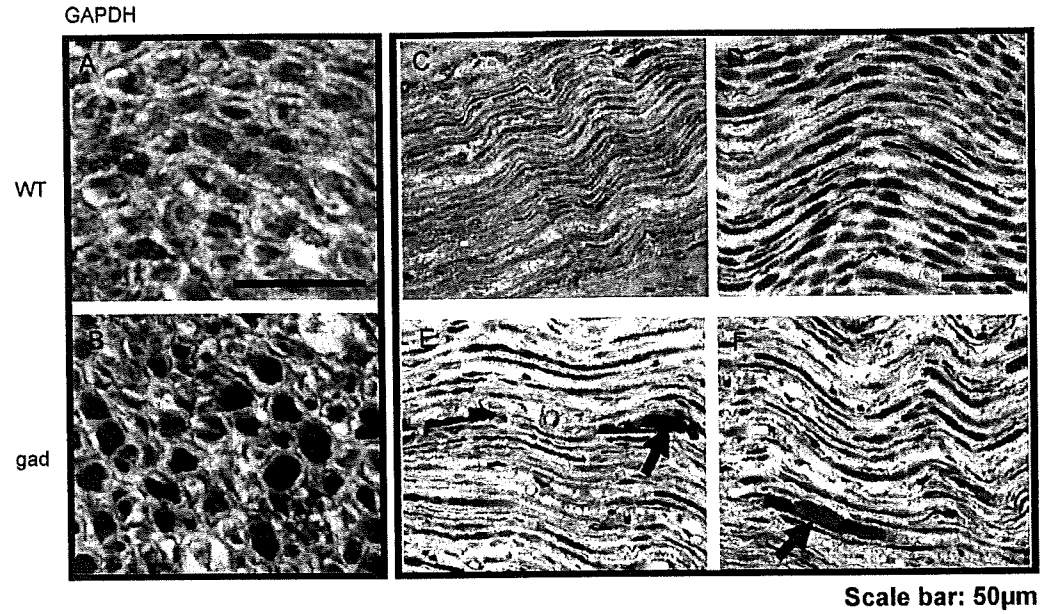

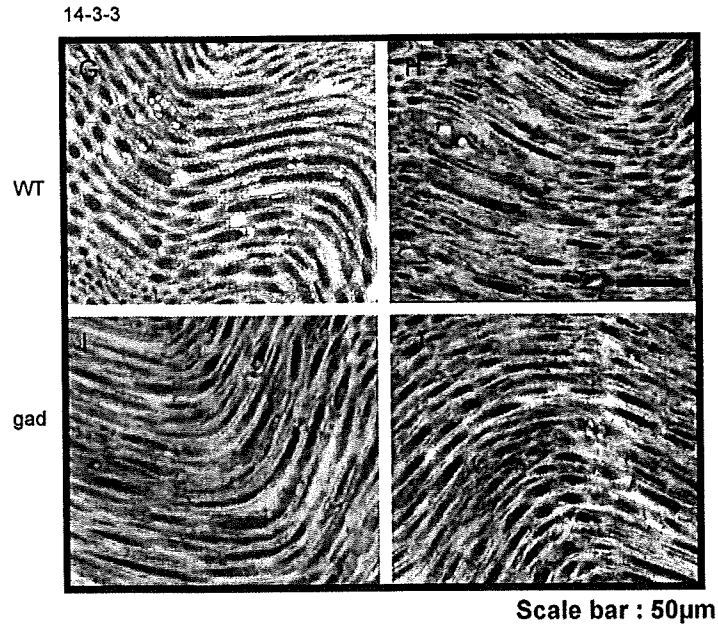

Fig. 4. DAB staining of GAPDH and 14-3-3 in the sciatic nerves of *gad* and WT mice.
(A–F) Sections of sciatic nerves of WT (A, C, and D) or *gad* (B, E, and F) mice stained with DAB using GAPDH antibodies.
(A) Cross-section of a sciatic nerve of a WT mouse. GAPDH is mainly localized in axons.
(B) Cross-section of a sciatic nerve of a *gad* mouse. GAPDH is mainly localized in axons and is highly expressed compared with the WT mouse.
(C and D) Vertical sections of sciatic nerves of WT mice. GAPDH is localized in axons.
(E and F) Vertical sections of sciatic nerves of *gad* mice. GAPDH is localized in axons and is accumulated. GAPDH aggregates are indicated by arrows.
(G–J) Sections of sciatic nerves of WT (G, H) and *gad* (I, J) mice stained with DAB using 14-3-3 antibodies.
(G and H) Vertical sections of sciatic nerves of WT mice; 14-3-3 is localized in axons of WT mice.
(I and J) Vertical sections of sciatic nerves of *gad* mice; 14-3-3 is localized in axons of *gad* mice, and there was no significant difference between *gad* and WT mice (G, H).

nerves of *gad* and WT mice. We found that although sulfonated GAPDH was not detected in WT mice, it was clearly detected in *gad* mice (Fig. 5A and B). In *gad* mice, sulfonated GAPDH was colocalized with the neuronal markers βTUBIII (Fig. 5B) and NF-M (data not shown) in axons. In *gad* mice, accumulated sulfonated GAPDH was also detected in the outer portion of the axons, around the DAPI staining for nuclei (Fig. 5C). Axons do not contain nuclei, so these DAPI signals may come from Schwann cells. The same results were obtained in 3 independent experiments.

3.7. Histological analyses of HNE, a marker of oxidative stress, in the sciatic nerves of gad and WT mice

The results shown in Fig. 5 suggest that the level of oxidative stress is increased in *gad* mice. Accordingly, we examined the existence of HNE, a major marker of oxidative stress, in addition to sulfonated GAPDH. HNE was detected in *gad* mice, but not in WT mice (Fig. 6). The same results were obtained in 3 independent experiments.

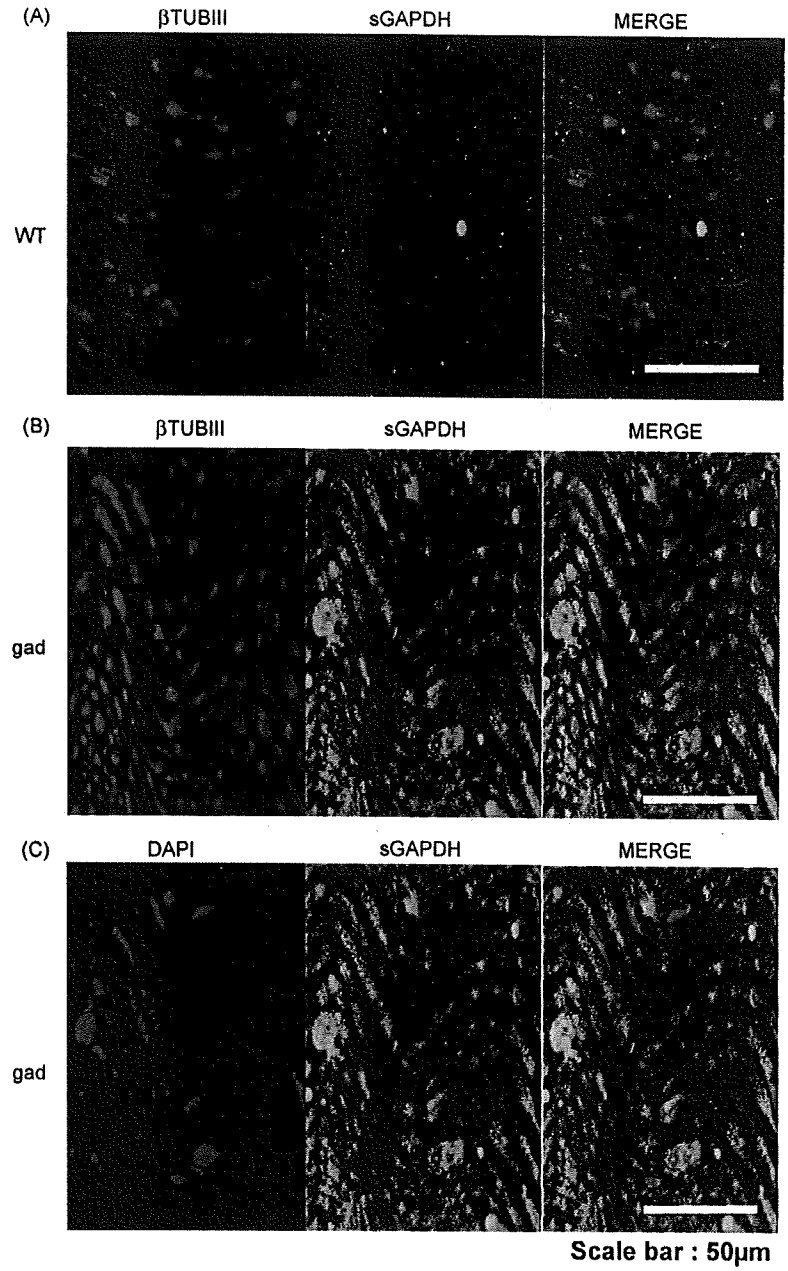

Fig. 5. Expression of sulfonated GAPDH in the sciatic nerves of *gad* and WT mice.
(A) Double immunofluorescent staining of a sciatic nerve of a WT mouse using antibodies against sulfonated GAPDH and βTUBIII. Sulfonated GAPDH was not detected in WT mice (middle panel).
(B) Double immunofluorescent staining of a sciatic nerve of a *gad* mouse using antibodies against sulfonated GAPDH and βTUBIII. In *gad* mice, sulfonated GAPDH was detected in axons of sciatic nerves (middle panel). Sulfonated GAPDH was colocalized with the neuronal marker βTUBIII in *gad* mice (right panel), as well as NF-M (data not shown). A representative result from 3 independent experiments is shown.
(C) Double immunofluorescent staining of a sciatic nerve of the *gad* mouse using an antibody against sulfonated GAPDH and DAPI. Sulfonated GAPDH was detected uniformaly within the axons of *gad* mice, and accumulation of sulfonated GAPDH was detected around the DAPI signals (right panel).

4. Discussion

In this study, we found that 14-3-3, annexin V, NF-L, and GAPDH were increased in an age-dependent manner in *gad* mice that display the dying-back-type of axonal degeneration, using 2D-DIGE analyses (Fig. 1). Based on Western blotting analyses, 14-3-3 and GAPDH were increased in *gad* mice compared with WT mice (Fig. 2). Histochemical analysis revealed that GAPDH was localized throughout axons and was accumulated in axons in *gad* mice compared with WT mice (Figs. 3 and 4). Also 14-3-3 was localized throughout axons, but there was no significant difference between *gad* and WT mice upon histochemical analyses, although it was increased in *gad* mice upon Western blotting analyses (Fig. 4). Since Western blotting showed only a slight increase in 14-3-3 (Fig. 2), we assume that this small difference could not be detected by histochemical analyses.

GAPDH is a classic glycolytic enzyme (Sirover, 1999; Chuang et al., 2005), and recent studies show that it is multifunctional

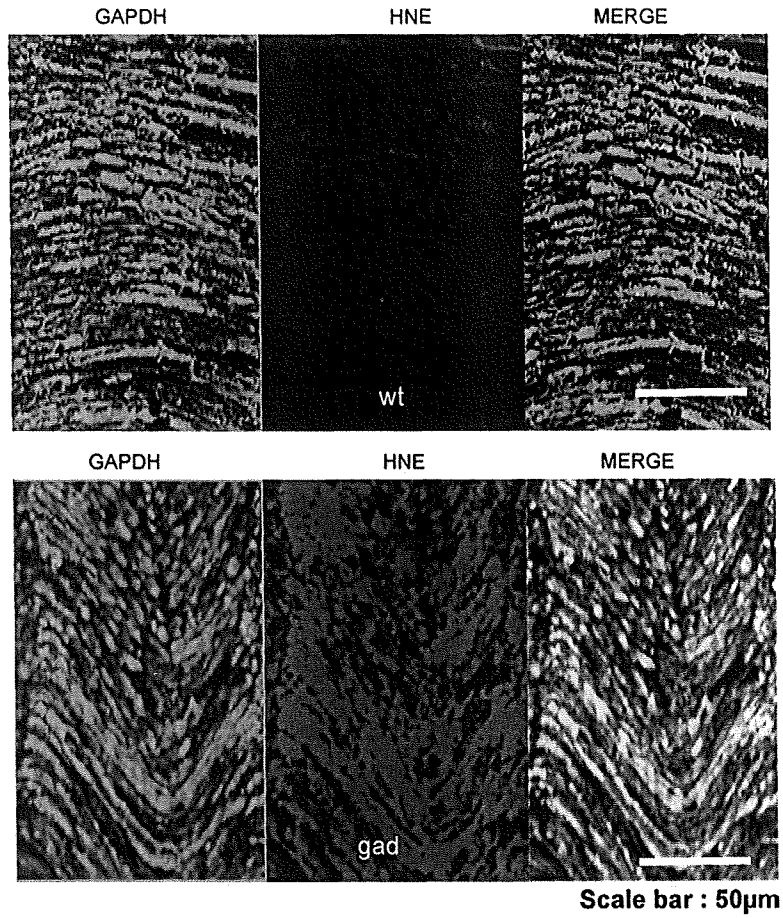

Fig. 6. Expression of HNE, a marker of oxidative stress, in the sciatic nerves of *gad* and WT mice.
Double immunofluorescent staining of sciatic nerves of *gad* and WT mice using antibodies against GAPDH and HNE. In WT mice, HNE was not detected (upper panel). On the other hand, HNE was strongly detected and mainly colocalized with GAPDH in *gad* mice (lower panel).

(Hara et al., 2006a). GAPDH has been reported to play roles in membrane fusion, microtubule bundling, nuclear RNA transport (Sirover, 1999), and transcription (Zheng et al., 2003). Particularly, its role as a mediator for cellular dysfunction/death has been highlighted (Sawa et al., 1997; Ishitani et al., 1998; Hara et al., 2005, 2006b). Sulfonation of GAPDH is reported to be induced by oxidative stress, and sulfonated GAPDH leads to cellular dysfunction (Hara et al., 2005, 2006a; Sen et al., 2008). Additionally, oxidative stress induces the oligomerization and aggregation of GAPDH through aberrant disulfide bonding of active-site cysteines, which leads to the formation of insoluble aggregates *in vitro* (Cumming and Schubert, 2005; Nakajima et al., 2007). Thus, GAPDH appears to participate in the mechanism leading to cellular dysfunction/death induced by oxidative stress. However, its function in axons or its association with axonal degeneration has not yet been demonstrated.

In this study, we found that GAPDH and sulfonated GAPDH were accumulated in *gad* mice compared with WT mice, suggesting that oxidative stress is increased in *gad* mice. In fact, we found that the oxidative stress marker HNE is increased in *gad* mice. It has also been reported that, the levels of carbonyl modification of proteins that is caused by oxidative stress are increased in the brains of *gad* mice compared with WT mice (Castegna et al., 2004). Therefore, we assume that accumulation of GAPDH and sulfonated GAPDH in the axons of *gad* mice were induced by oxidative stress.

Various molecules are involved in reduction-oxidative reactions, and recently the necessity of the UPS in reduction-oxidative reactions has been highlighted (Okada et al., 1999; Kang et al., 2008). It has been reported that a number of oxidative stress sensors are regulated by the UPS (Iwai, 2003; Kobayashi et al., 2004; Hara et al., 2006a). In *gad* mice, free-Ub pools are decreased in neurons, and proteolysis in the UPS is thought to be abnormal (Osaka et al., 2003). Oxidative stress is therefore expected to be increased in *gad* mice, which is consistent with our findings.

There is another possible mechanism for the accumulation of GAPDH in the axons of *gad* mice. GAPDH is reported to be degraded mainly by chaperone-mediated autophagy (Aniento et al., 1993; Cuervo et al., 1997). Our recent study showed that UCH-L1 physically interacts with lysosome-associated membrane protein type 2A, which is a component of CMA (Kabuta et al., 2008); thus CMA is possibly altered in the neuronal system of *gad* mice, potentially leading to the accumulation of GAPDH in the axons of *gad* mice.

This study demonstrates the alteration of GAPDH in axons of the *gad* mouse, a mutant with a loss of function of UCH-L1. Our findings suggest that GAPDH may participate in the process leading to the dying-back-type of axonal degeneration in *gad* mice and may provide valuable insight into the mechanisms of axonal degeneration.

Acknowledgements

We thank the following people for their contributions to this work: Dr. Hidemitsu Nakajima (Osaka Prefecture University), Dr. Satoshi Nagamine (National Center of Neurology and Psychiatry) and Dr. Makoto R. Hara (Johns Hopkins University School of Medicine) for helpful discussions; Ms. Hisae Kikuchi (National Center of Neurology and Psychiatry) for technical assistance with tissue sections; Ms. Masako Shikama (National Center of Neurology and Psychiatry) for the care and breeding of animals; Dr. Hayato Onishi (University of Tokyo) for assistance with the TOF MASS analysis; and Dr. H. Akiko Popiel (National Center of Neurology and Psychiatry) for support with English; Mitsubishi Tanabe Pharma Corporation for giving a chance to A.G. of admission to doctoral course. This work was supported in part by Grants-in-Aid for Scientific Research from the Ministry of Health, Labour and Welfare of Japan, Grants-in-Aid for Scientific Research from the Ministry of Education, Culture, Sports, Science and Technology of Japan, the Program for Promotion of Fundamental Studies in Health Sciences of the National Institute of Biomedical Innovation, and a grant from Japan Science and Technology Agency.

References

Aniento, F., Roche, E., Cuervo, A.M., Knecht, E., 1993. Uptake and degradation of glyceraldehyde-3-phosphate dehydrogenase by rat liver lysosomes. J. Biol. Chem. 268, 10463–10470.

Castegna, A., Thongboonkerd, V., Klein, J., Lynn, B.C., Wang, Y.L., Osaka, H., Wada, K., Butterfield, D.A., 2004. Proteomic analysis of brain proteins in the gracile axonal dystrophy (gad) mouse, a syndrome that emanates from dysfunctional ubiquitin carboxyl-terminal hydrolase L-1, reveals oxidation of key proteins. J. Neurochem. 88, 1540–1546.

Chuang, D.M., Hough, C., Senatorov, V.V., 2005. Glyceraldehyde-3-phosphate dehydrogenase, apoptosis, and neurodegenerative diseases. Annu. Rev. Pharmacol. Toxicol. 45, 269–290.

Cuervo, A.M., Dice, J.F., Knecht, E., 1997. A population of rat liver lysosomes responsible for the selective uptake and degradation of cytosolic proteins. J. Biol. Chem. 272, 5606–5615.

Cumming, R.C., Schubert, D., 2005. Amyloid-beta induces disulfide bonding and aggregation of GAPDH in Alzheimer's disease. FASEB J. 19, 2060–2062.

Ferri, A., Sanes, J.R., Coleman, M.P., Cunningham, J.M., Kato, A.C., 2003. Inhibiting axon degeneration and synapse loss attenuates apoptosis and disease progression in a mouse model of motoneuron disease. Curr. Biol. 13, 669–673.

Fischer, L.R., Culver, D.G., Tennant, P., Davis, A.A., Wang, M., Castellano-Sanchez, A., Khan, J., Polak, M.A., Glass, J.D., 2004. Amyotrophic lateral sclerosis is a distal axonopathy: evidence in mice and man. Exp. Neurol. 185, 232–240.

Fischer, L.R., Glass, J.D., 2007. Axonal degeneration in motor neuron disease. Neurodegener. Dis. 4, 431–442.

Hara, M.R., Agrawal, N., Kim, S.F., Cascio, M.B., Fujimuro, M., Ozeki, Y., Takahashi, M., Cheah, J.H., Tankou, S.K., Hester, L.D., Ferris, C.D., Hayward, S.D., Snyder, S.H., Sawa, A., 2005. S-nitrosylated GAPDH initiates apoptotic cell death by nuclear translocation following Siah1 binding. Nat. Cell. Biol. 7, 665–674.

Hara, M.R., Cascio, M.B., Sawa, A., 2006a. GAPDH as a sensor of NO stress. Biochim. Biophys. Acta 1762, 502–509.

Hara, M.R., Thomas, B., Cascio, M.B., Bae, B.I., Hester, L.D., Dawson, V.L., Dawson, T.M., Sawa, A., Snyder, S.H., 2006b. Neuroprotection by pharmacologic blockade of the GAPDH death cascade. Proc. Natl. Acad. Sci. U.S.A. 103, 3887–3889.

Harada, T., Harada, C., Wang, Y.L., Osaka, H., Amanai, K., Tanaka, K., Takizawa, S., Setsuie, R., Sakurai, M., Sato, Y., Noda, M., Wada, K., 2004. Role of ubiquitin carboxy terminal hydrolase-L1 in neural cell apoptosis induced by ischemic retinal injury in vivo. Am. J. Pathol. 164, 59–64.

Ishitani, R., Tanaka, M., Sunaga, K., Katsube, N., Chuang, D.M., 1998. Nuclear localization of overexpressed glyceraldehyde-3-phosphate dehydrogenase in cultured cerebellar neurons undergoing apoptosis. Mol. Pharmacol. 53, 701–707.

Iwai, K., 2003. An ubiquitin ligase recognizing a protein oxidized by iron: implications for the turnover of oxidatively damaged proteins. J. Biochem. 134, 175–182.

Kabuta, T., Furuta, A., Aoki, S., Furuta, K., Wada, K., 2008. Aberrant interaction between Parkinson disease-associated mutant UCH-L1 and the lysosomal receptor for chaperone-mediated autophagy. J. Biol. Chem. 283, 23731–23738.

Kang, S.I., Choi, H.W., Kim, I.Y., 2008. Redox-mediated modification of PLZF by SUMO-1 and ubiquitin. Biochem. Biophys. Res. Commun. 369, 1209–1214.

Kikuchi, T., Mukoyama, M., Yamazaki, K., Moriya, H., 1990. Axonal degeneration of ascending sensory neurons in gracile axonal dystrophy mutant mouse. Acta Neuropathol. 80, 145–151.

Knowles, M.R., Cervino, S., Skynner, H.A., Hunt, S.P., de Felipe, C., Salim, K., Meneses-Lorente, G., McAllister, G., Guest, P.C., 2003. Multiplex proteomic analysis by two-dimensional differential in-gel electrophoresis. Proteomics 3, 1162–1171.

Kobayashi, A., Kang, M.I., Okawa, H., Ohtsuji, M., Zenke, Y., Chiba, T., Igarashi, K., Yamamoto, M., 2004. Oxidative stress sensor Keap1 functions as an adaptor for Cul3-based E3 ligase to regulate proteasomal degradation of Nrf2. Mol. Cell. Biol. 24, 7130–7139.

Larsen, C.N., Krantz, B.A., Wilkinson, K.D., 1998. Substrate specificity of deubiquitinating enzymes: ubiquitin C-terminal hydrolases. Biochemistry 37, 3358–3368.

Li, H., Li, S.H., Yu, Z.X., Shelbourne, P., Li, X.J., 2001. Huntingtin aggregate-associated axonal degeneration is an early pathological event in Huntington's disease mice. J. Neurosci. 21, 8473–8481.

Liu, Y., Fallon, L., Lashuel, H.A., Liu, Z., Lansbury Jr., P.T., 2002. The UCH-L1 gene encodes two opposing enzymatic activities that affect alpha-synuclein degradation and Parkinson's disease susceptibility. Cell 111, 209–218.

Miura, H., Oda, K., Endo, C., Yamazaki, K., Shibasaki, H., Kikuchi, T., 1993. Progressive degeneration of motor nerve terminals in GAD mutant mouse with hereditary sensory axonopathy. Neuropathol. Appl. Neurobiol. 19, 41–51.

Mukoyama, M., Yamazaki, K., Kikuchi, T., Tomita, T., 1989. Neuropathology of gracile axonal dystrophy (GAD) mouse. An animal model of central distal axonopathy in primary sensory neurons. Acta Neuropathol. 79, 294–299.

Nakajima, H., Amano, W., Fujita, A., Fukuhara, A., Azuma, Y.T., Hata, F., Inui, T., Takeuchi, T., 2007. The active site cysteine of the proapoptotic protein glyceraldehyde-3-phosphate dehydrogenase is essential in oxidative stress-induced aggregation and cell death. J. Biol. Chem. 282, 26562–26574.

Oda, K., Yamazaki, K., Miura, H., Shibasaki, H., Kikuchi, T., 1992. Dying back type axonal degeneration of sensory nerve terminals in muscle spindles of the gracile axonal dystrophy (GAD) mutant mouse. Neuropathol. Appl. Neurobiol. 18, 265–281.

Okada, K., Wangpoengtrakul, C., Osawa, T., Toyokuni, S., Tanaka, K., Uchida, K., 1999. 4-Hydroxy-2-nonenal-mediated impairment of intracellular proteolysis during oxidative stress. Identification of proteasomes as target molecules. J. Biol. Chem. 274, 23787–23793.

Osaka, H., Wang, Y.L., Takada, K., Takizawa, S., Setsuie, R., Li, H., Sato, Y., Nishikawa, K., Sun, Y.J., Sakurai, M., Harada, T., Hara, Y., Kimura, I., Chiba, S., Namikawa, K., Kiyama, H., Noda, M., Aoki, S., Wada, K., 2003. Ubiquitin carboxy-terminal hydrolase L1 binds to and stabilizes monoubiquitin in neuron. Hum. Mol. Genet. 12, 1945–1958.

Saigoh, K., Wang, Y.L., Suh, J.G., Yamanishi, T., Sakai, Y., Kiyosawa, H., Harada, T., Ichihara, N., Wakana, S., Kikuchi, T., Wada, K., 1999. Intragenic deletion in the gene encoding ubiquitin carboxy-terminal hydrolase in gad mice. Nat. Genet. 23, 47–51.

Sawa, A., Khan, A.A., Hester, L.D., Snyder, S.H., 1997. Glyceraldehyde-3-phosphate dehydrogenase: nuclear translocation participates in neuronal and nonneuronal cell death. Proc. Natl. Acad. Sci. U.S.A. 94, 11669–11674.

Sen, N., Hara, M.R., Kornberg, M.D., Cascio, M.B., Bae, B.I., Shahani, N., Thomas, B., Dawson, T.M., Dawson, V.L., Snyder, S.H., Sawa, A., 2008. Nitric oxide-induced nuclear GAPDH activates p300/CBP and mediates apoptosis. Nat. Cell. Biol. 10, 866–873.

Shaw, M.M., Riederer, B.M., 2003. Sample preparation for two-dimensional gel electrophoresis. Proteomics 3, 1408–1417.

Sirover, M.A., 1999. New insights into an old protein: the functional diversity of mammalian glyceraldehyde-3-phosphate dehydrogenase. Biochim. Biophys. Acta 1432, 159–184.

Stokin, G.B., Lillo, C., Falzone, T.L., Brusch, R.G., Rockenstein, E., Mount, S.L., Raman, R., Davies, P., Masliah, E., Williams, D.S., Goldstein, L.S., 2005. Axonopathy and transport deficits early in the pathogenesis of Alzheimer's disease. Science 307, 1282–1288.

Wang, Y.L., Takeda, A., Osaka, H., Hara, Y., Furuta, A., Setsuie, R., Sun, Y.J., Kwon, J., Sato, Y., Sakurai, M., Noda, M., Yoshikawa, Y., Wada, K., 2004. Accumulation of beta- and gamma-synucleins in the ubiquitin carboxyl-terminal hydrolase L1-deficient gad mouse. Brain Res. 1019, 1–9.

Wilkinson, K.D., Lee, K.M., Deshpande, S., Duerksen-Hughes, P., Boss, J.M., Pohl, J., 1989. The neuron-specific protein PGP 9.5 is a ubiquitin carboxyl-terminal hydrolase. Science 246, 670–673.

Yamazaki, K., Wakasugi, N., Tomita, T., Kikuchi, T., Mukoyama, M., Ando, K., 1988. Gracile axonal dystrophy (GAD), a new neurological mutant in the mouse. Proc. Soc. Exp. Biol. Med. 187, 209–215.

Zheng, L., Roeder, R.G., Luo, Y., 2003. S phase activation of the histone H2B promoter by OCA-S, a coactivator complex that contains GAPDH as a key component. Cell 114, 255–266.

De novo mutations of voltage-gated sodium channel α_{II} gene *SCN2A* in intractable epilepsies

I. Ogiwara, PhD
K. Ito, PhD
Y. Sawaishi, MD, PhD
H. Osaka, MD, PhD
E. Mazaki, MS
I. Inoue, MS
M. Montal, MD, PhD
T. Hashikawa, PhD
T. Shike, MD
T. Fujiwara, MD, PhD
Y. Inoue, MD, PhD
M. Kaneda, MD, PhD
K. Yamakawa, PhD

Address correspondence and reprint requests to Dr. Kazuhiro Yamakawa, Laboratory for Neurogenetics, RIKEN Brain Science Institute, 2-1 Hirosawa, Wako, Saitama 351-0198, Japan
yamakawa@brain.riken.jp

ABSTRACT

Background: Mutations of voltage-gated sodium channel α_{II} gene, *SCN2A*, have been described in a wide spectrum of epilepsies. While inherited *SCN2A* mutations have been identified in multiple mild epilepsy cases, a de novo *SCN2A*-R102X mutation, which we previously reported in a patient with sporadic intractable childhood localization-related epilepsy, remains unique. To validate the involvement of de novo SCN2A mutations in the etiology of intractable epilepsies, we sought to identify additional instances.

Methods: We performed mutational analyses on *SCN2A* in 116 patients with severe myoclonic epilepsy in infancy, infantile spasms, and other types of intractable childhood partial and generalized epilepsies and did whole-cell patch-clamp recordings on $Na_v1.2$ channels containing identified mutations.

Results: We discovered 2 additional de novo SCN2A mutations. One mutation, *SCN2A*-E1211K, was identified in a patient with sporadic infantile spasms. *SCN2A*-E1211K produced channels with altered electrophysiologic properties compatible with both augmented (a ~18-mV hyperpolarizing shift in the voltage dependence of activation) and reduced (a ~22-mV hyperpolarizing shift in the voltage dependence of steady-state inactivation and a slowed recovery from inactivation) channel activities. The other de novo mutation, *SCN2A*-I1473M, was identified in a patient with sporadic neonatal epileptic encephalopathy. *SCN2A*-I1473M caused a ~14-mV hyperpolarizing shift in the voltage dependence of activation.

Conclusions: The identified de novo mutations *SCN2A*-E1211K, -I1473M, and -R102X indicate that *SCN2A* is an etiologic candidate underlying a variety of intractable childhood epilepsies. The phenotypic variations among patients might be due to the different electrophysiologic properties of mutant channels. ***Neurology*® 2009;73:1046-1053**

GLOSSARY

BFNIS = benign familial neonatal-infantile seizures; **EMA** = epilepsy with myoclonic absence; **FLE** = frontal lobe epilepsy; **GEFS+** = generalized epilepsy with febrile seizures plus; **IS** = infantile spasms; **OLE** = occipital lobe epilepsy; **PE** = partial epilepsy; **SMEB** = borderline severe myoclonic epilepsy in infancy; **SMEI** = severe myoclonic epilepsy in infancy; **VGSC** = voltage-gated sodium channel; **WT** = wild-type.

Voltage-gated sodium channels (VGSCs) are essential for the action potential generation and propagation in brain, muscle, and heart. VGSCs consist of 1 α pore-forming main subunit and 1 or 2 β accessory subunits that modulate the voltage dependence and cellular localization of the α subunit. Four α subunits (α_{I-III} and $_{VI}$) and 4 β subunits (β_{I-IV}) are highly expressed in human brain. Mutations in the brain-type VGSC α_I, α_{II}, and β_I genes have been described in multiple epileptic disorders.[1,2]

Mutations in VGSC α_I gene, *SCN1A*, encoding $Na_v1.1$, have been reported in generalized epilepsy with febrile seizures plus (GEFS+: OMIM no. 604233), severe myoclonic epilepsy in

Supplemental data at www.neurology.org

From the Laboratories for Neurogenetics (I.O., K.I., E.M., I.I., M.K., K.Y.) and Neural Architecture (T.H.), RIKEN Brain Science Institute, Wako; Department of Comparative Pathophysiology (K.I.), Graduate School of Agricultural and Life Sciences, the University of Tokyo; Department of Pediatrics (Y.S.), Akita University School of Medicine; Division of Neurology (H.O.), Kanagawa Children's Medical Center, Japan; Section of Neurobiology (M.M.), Division of Biological Sciences, University of California San Diego; National Epilepsy Center (T.S., Y.I., F.T.), Shizuoka Institute of Epilepsy and Neurological Disorders; and Department of Physiology (M.K.), Keio University School of Medicine, Japan.

Supported by grants from the RIKEN Brain Science Institute, the Ministry of Health, Labour and Welfare of Japan, the Ministry of Education, Culture, Sports, Science and Technology of Japan, and the NIH (GM-49711).

Disclosure: The authors report no disclosures.

infancy (SMEI or Dravet syndrome; OMIM no. 607208), and borderline SMEI (SMEB), including intractable childhood epilepsy with generalized tonic-clonic seizures.[3-8] GEFS+ is a dominantly inherited epilepsy characterized by febrile seizures in early childhood that progress to afebrile seizures in late childhood and is responsive to antiepileptic drugs.[9] By contrast, SMEI is a severe and intractable infantile epilepsy. Typically, the first seizure in SMEI is most often a unilateral or generalized tonic-clonic or clonic seizure often associated with fever, which is progressively followed by additional generalized and partial seizures, ataxia, and mental decline.[10] Most SMEI cases occurred sporadically and are associated with de novo *SCN1A* mutations. *SCN1A* mutations have also been documented in a broad spectrum of early childhood intractable epilepsies including infantile spasms, myoclonic-astatic epilepsy, Lennox-Gastaut syndrome, and other forms of early childhood focal and generalized epilepsies. While *SCN1A* is the major and thus far the best characterized responsible gene for cryptogenic intractable childhood epilepsies, other candidate genes underlying *SCN1A*-negative cases remain largely unknown.[11,12]

We previously discovered a mutation of VGSC α_{II} gene *SCN2A*, encoding $Na_v1.2$, in a family with atypical GEFS+.[13] Other groups subsequently reported several other *SCN2A* mutations in families with benign familial neonatal-infantile seizures (BFNIS; OMIM no. 607745), which is as mild as GEFS+.[14-17] In addition to these inherited *SCN2A* mutations in mild epilepsies, we previously described a de novo nonsense mutation, *SCN2A*-R102X, in a patient with sporadic intractable childhood localization-related epilepsy associated with severe mental decline.[18] To date, *SCN2A*-R102X mutation still remains as a single case with sporadic intractable epilepsy. We hypothesized that other de novo SCN2A mutations occur, with altered electrophysiologic properties, and their existence would validate their pathophysiologic role in intractable epilepsies.

METHODS Patients. Ethics Committees in Akita University School of Medicine, the Shizuoka Institute of Epilepsy and Neurological Disorders, Kanagawa Children's Medical Center, and RIKEN Institute approved this study. Each adult participant or, where necessary, responsible guardians of adult subjects, as well as the parents or legal guardians of subjects who were minors at the time the study began, signed an informed consent form as approved by the Ethics Committees.

Proband 1. The proband (figure 1A; II-1) is a 22-year-old man. There are no close relatives with a history of epilepsy or febrile convulsion or other neuropsychiatric disorders. He was born by cesarean section at 41st week of gestation with mild asphyxia due to meconium aspiration. Birth weight was 3,000 g. He showed marked developmental delay and severe intellectual disability: he stood alone at age 7 years and spoke only 1 word. He started to have daily seizures at age 11 months with series of spasms (face frowning, body stiffening, then raising both upper limbs for 1–2 seconds), and was diagnosed with infantile spasms. At age 11 months and age 2 years, he received adrenocorticotropic hormone with cessation of seizures, although transiently. At age 2–3 years, infantile spasms evolved to tonic seizures, with extension of both upper arms occasionally accompanied by short clonic movements. Seizures were refractory to various conventional medications including valproate, phenobarbital, phenytoin, and clobazam. The seizure duration was for 10–20 seconds and the frequency of seizure attacks was 1 to 10 times per day, both during sleep and awake, especially frequently when falling asleep and during afternoon nap. After age 10 years, seizures were often triggered by fever above 37.5°C. No myoclonic seizures or absence seizures were observed. At age 17 years, he was brought to a hospital because of status epilepticus, which caused respiratory arrest necessitating tracheotomy. Thereafter, he became quadriplegic and speechless. At present, he has daily tonic seizures rarely followed by clonic movement and occasional status epilepticus. The recent EEG recording showed the background activity lacking alpha waves but containing abundant slow waves. There was no photo-paroxysmal response. Right hemisphere dominant diffuse sharp waves or polyspikes were seen. Ictal EEG showed diffuse recruiting fast spike activity preceded by diffuse flattening. MRI showed mild cerebral atrophy with wider lateral ventricle of the left side. SPECT showed no remarkable findings.

Proband 2. The proband (figure 1B; II-1) was a girl with unusual neonatal epileptic encephalopathy and the only member of her family with epilepsy. Her clinical details were described previously.[19] She had experienced tonic or tonic-clonic seizures from age 1 month. Other characteristic clinical features were loss of reactivity, a highly suppressed EEG with ictal burst activities, hyponatremia (120–130 mEq/L), and megalencephaly. She was partially rescued using lidocaine with the least effective serum concentration being 0.5 mg/L (2.1×10^{-6}M). At age 7 years and 8 months, she died from unknown causes at her home.

Mutational analysis. Mutational analyses of *SCN2A* in patients were performed on all of the 26 coding exons and exon-intron boundary regions as described previously.[13]

Haplotype analysis. The microsatellite markers flanking the *SCN2A* locus, D2S151, D2S2330, and D2S335, were genotyped using ABI PRISM Linkage Mapping Set v2.5 (PE Applied Biosystems, Foster City, CA) according to the manufacturer's instructions.

Construction of wild-type and mutant $Na_v1.2$ expression vectors. The wild-type human $Na_v1.2$ expression vector, phSCN2A_WT, has been described previously.[18] The mutant

Figure 1 Novel *SCN2A* nucleotide changes leading to amino acid substitutions identified in patients with intractable childhood epilepsies

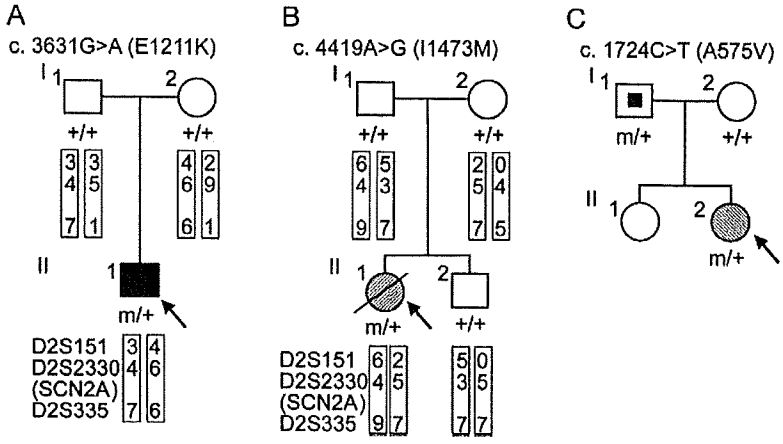

(A) Pedigree for proband 1 (II-1) with a history of infantile spasms that evolved to symptomatic generalized epilepsy who showed the nucleotide change c.3631C>T (E1211K). The putative haplotypes determined by analyzing microsatellite markers, namely, D2S151, D2S2330, and D2S335, flanking the *SCN2A* locus are shown. Markers are given in order, from the p telomere to the q telomere. + = Wild-type allele; m = mutated allele; filled square = infantile spasms. (B) Pedigree for proband 2 (II-1) with neonatal epileptic encephalopathy who showed the nucleotide change c.4419A>G (I1473M). The putative haplotypes determined by analyzing microsatellite markers flanking the *SCN2A* locus are shown. Genetic recombination occurred in the proband's or her brother's maternal chromosome within the region between D2S151 and D2S2330. + = Wild-type allele, m = mutated allele; hatched circle = neonatal epileptic encephalopathy; slash = deceased. (C) Pedigree for proband 3 (II-2) with SMEB who showed the nucleotide change c.1724C>T (A575V). The nucleotide change was also detected in her asymptomatic father. Genomic DNA of her sister was not available for the analysis. + = Wild-type allele; m = mutated allele; hatched circle = SMEB; symbol with a dot = asymptomatic mutation carrier.

vectors, phSCN2A_E1211K, phSCN2A_I1473M, and phSCN2A_A575V, were generated from phSCN2A_WT using QuikChange Mutagenesis kit (Stratagene, LA Jolla, CA) according to the manufacturer's instructions. All constructs were verified by sequencing and confirmed not to contain any unwanted substitutions.

Cell culture and transfection. Human embryonic kidney HEK293 cells were plated on polylysine-coated 6-well dishes and then transfected with phSCN2A_WT, phSCN2A_E1211K, phSCN2A_I1473M, or phSCN2A_A575V together with phSCN1B-IRES2-EGFP and phSCN2B-IRES2-EGFP using Lipofectamine LTX (Invitrogen, Carlsbad, CA) according to the manufacturer's instructions.

Patch-clamp analysis. Patch-clamp analysis was performed as described previously.[18] Using Eclipse FN1 upright microscope (Nikon, Tokyo Japan), cells were selected by their fluorescence. Currents were recorded using Axopatch 200B amplifier (Axon Instruments, Burlingame, CA). All experiments were carried out at room temperature (22°C). Recordings from cells showing peak currents less than 200 pA were excluded from the analysis in order to eliminate any potential contribution from the small (~50 pA) Na^+ currents present in a fraction of untransfected HEK293 cells. The electrophysiologists performing all experimental recordings were blinded to the HEK293 cell genotypes used. Data are given as mean ± SEM. Differences were considered significant using Student *t* test if $p < 0.05$.

RESULTS Novel *SCN2A* missense mutations in patients with intractable childhood epilepsies. We performed mutational analyses on *SCN2A* in 116 patients with intractable childhood epilepsies. These patients were negative for *SCN1A* mutations. The cohort consisted of 19, 25, 3, 3, 2, 2, 47, and 15 patients presenting SMEI, SMEB, infantile spasms, occipital lobe epilepsy, frontal lobe epilepsy, epilepsy with myoclonic absence, and unclassified partial epilepsies and unclassified generalized epilepsies. In the cohort, we found a total of 6 different nucleotide changes leading to amino acid substitutions in *SCN2A* (table). Among these nucleotide changes, c.3631G>A (E1211K), c.4419A>G (I1473M), c.1724C>T (A575V), and c.982T>G (F328V) were novel. E1211K, I1473M, and A575V were observed only in affected individuals but not in our pool of healthy controls (312 or 311 individuals), and therefore were subjected to further whole-cell patch-clamp recordings as described below. F328V was found in patients and healthy controls and therefore conjectured to be nonpathogenic. The other 2 nucleotide changes, c.56G>A (R19K) and c.1571G>A (R524Q), were previously reported to produce unre-

Table Nucleotide changes leading to amino acid substitutions in *SCN2A*

	Frequency in patients								
							Unclassified		
Nucleotide changes (amino acid substitutions)	SMEI	SMEB	IS	OLE	FLE	EMA	PE	GE	Frequency in healthy controls
c.3631G>A (E1211K)	0/19	0/25	1/3	0/3	0/2	0/2	0/47	0/15	0/312
c.4419A>G (I1473M)	0/19	0/25	0/3	0/3	0/2	0/2	0/47	1/15	0/311
c.1724C>T (A575V)	0/19	1/25	0/3	0/3	0/2	0/2	0/47	0/15	0/311
c.982T>G (F328V)	1/19	0/25	0/3	0/3	0/2	0/2	1/47	0/15	2/309
c.1571G>A (R524Q)	0/19	0/25	0/3	0/3	0/2	0/2	0/47	1/15	1/164[13]
c.56G>A (R19K)	4/19	0/25	0/3	0/3	0/2	0/2	7/47	1/15	9/112[13]

SMEI = severe myoclonic epilepsy in infancy; SMEB = borderline severe myoclonic epilepsy in infancy; IS = infantile spasms; OLE = occipital lobe epilepsy; FLE = frontal lobe epilepsy; EMA = epilepsy with myoclonic absence; PE = partial epilepsy; GE = generalized epilepsy.

Figure 2 *SCN2A* nucleotide changes leading to amino acid substitutions detected in intractable childhood epilepsies

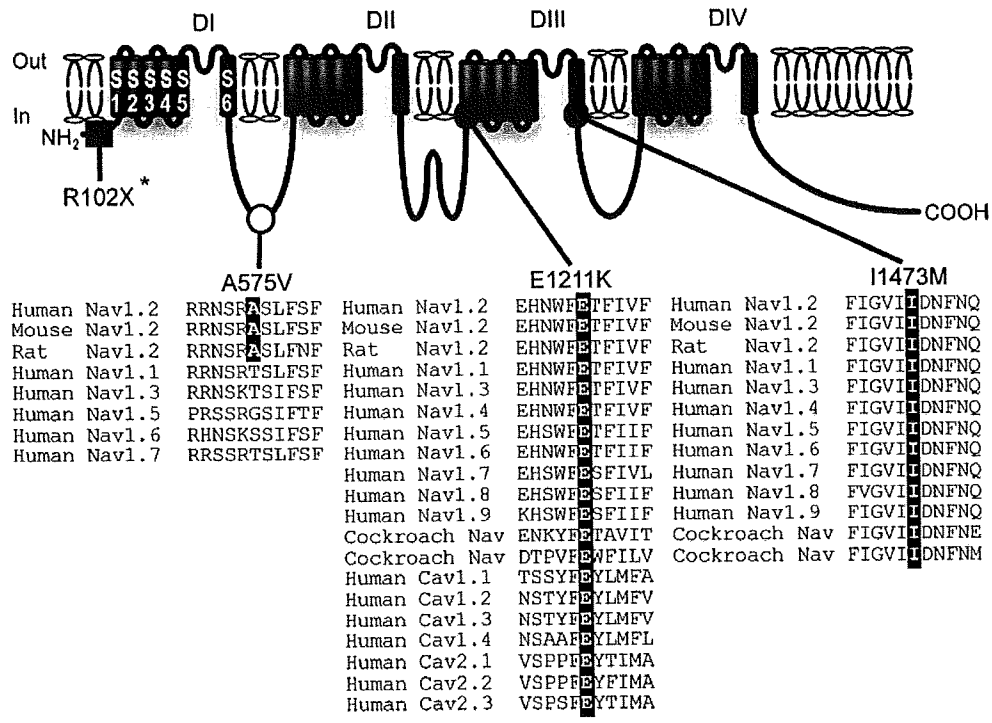

An asterisk indicates a nonsense mutation, *SCN2A*-R102X, described before.[18] *SCN2A*-A575V is assigned to the intracellular linker between domain I (DI) and DII. The alanine residue A575 (highlighted in black) is conserved among human, mouse, and rat $Na_v1.2$ but not in other types of mammalian VGSC α subunits. *SCN2A*-E1211K is localized to transmembrane segment 1 (S1) of DIII. The glutamate residue E1211 (highlighted in black) is significantly conserved through vertebrate and invertebrate VGSC α subunits and human calcium channel α subunits. I1473M is localized to S6 of DIII. The isoleucine residue I1473 (highlighted in black) is perfectly conserved through vertebrate and invertebrate sodium channel α subunits. Filled square = de novo nonsense mutation; filled circle = de novo missense mutation; open circle = possible nonpathogenic variant. Sources of amino acid sequences are as follows (notations refer to accession numbers): Human $Na_v1.2$, NP_001035232; mouse $Na_v1.2$, NP_001092768; rat $Na_v1.2$, NP_036779; human $Na_v1.1$, NP_008851; human $Na_v1.3$, NP_008853; human $Na_v1.4$, NP_000325; human $Na_v1.5$, NP_932173; human $Na_v1.6$, NP_055006; human $Na_v1.7$, NP_002968; human $Na_v1.8$, NP_006505; human $Na_v1.9$, NP_054858; cockroach sodium channels, AAC47483 and AAK01090; human $Ca_v1.1$, NP_000060; human $Ca_v1.2$, NP_000719; human $Ca_v1.3$, NP_000711; human $Ca_v1.4$, NP_005174; human $Ca_v2.1$, NP_000059; human $Ca_v2.2$, NP_000709; human $Ca_v2.3$, NP_000712.

markable changes of the electrophysiologic properties of rat $Na_v1.2$ and therefore assigned as nonpathogenic variants.[13]

E1211K and I1473M are de novo mutations whereas A575V is inherited. E1211K was found in the proband 1 with infantile spasms that evolved to severe symptomatic generalized epilepsy of a tonic seizure phenotype (figure 1A and figure e-1A [on the *Neurology*® Web site at www.neurology.org]; see Methods for the patient's clinical details). E1211K was not detected in his asymptomatic parents and therefore was defined as a de novo mutation in the proband. The putative haplotypes determined by analyzing the microsatellite markers flanking the *SCN2A* locus support their genetic kinship.

I1473M was found in the proband 2 with sporadic neonatal epileptic encephalopathy, which was categorized as unclassified generalized epilepsy in the table (figure 1B and figure e-1B). The clinical features were similar but distinct from those of early infantile epileptic encephalopathy with suppression burst (also known as Ohtahara syndrome).[19] I1473M was a de novo mutation in the proband because it was not detected in her asymptomatic parents. The putative haplotypes determined by analyzing the microsatellite markers flanking the *SCN2A* locus support their genetic kinship.

A575V was found in the proband 3 with SMEB (figure 1C and figure e-1C; see e-Methods for the patient's clinical details). A575V was also found in her asymptomatic father.

E1211 and I1473 are evolutionarily conserved among vertebrate and invertebrate VGSC α subunits. The glutamate residue of *SCN2A*-E1211K putatively located on transmembrane segment 1 (S1) of domain III (DIII) was highly conserved among vertebrate

Figure 3 **Voltage-gated Na^+ currents recorded from HEK293 cells expressing human wild-type and mutant (E1211K, I1473M, and A575V) $Na_v1.2$ channels**

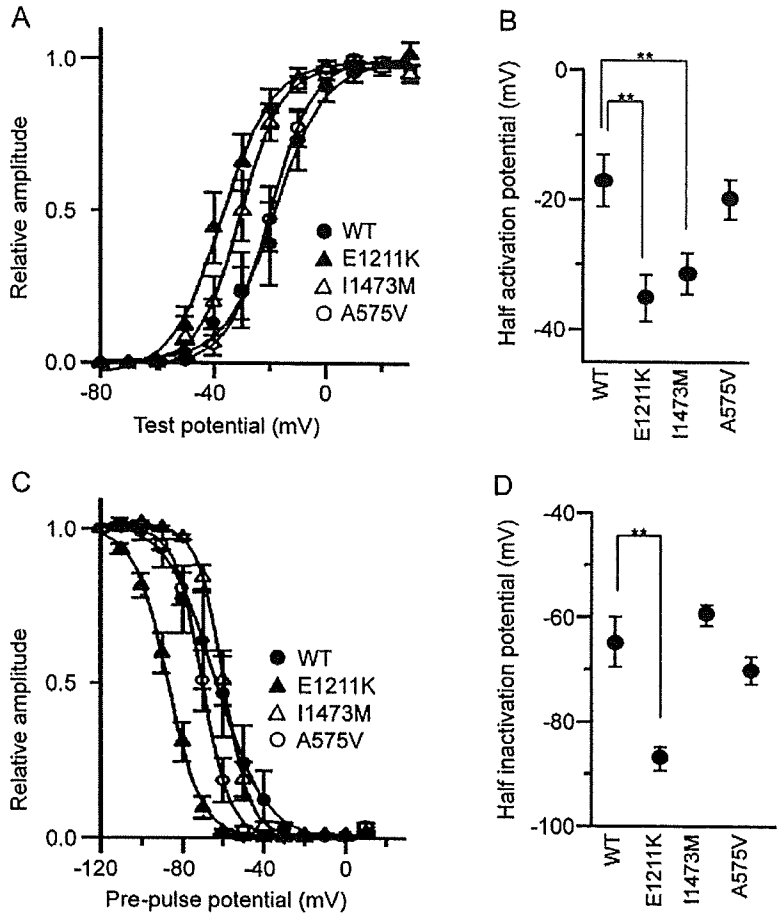

(A) Peak sodium conductance-voltage relationships for wild-type (WT; closed circle), E1211K (closed triangle), I1473M (open triangle), and A575V (open circle). Na^+ currents were evoked by 10 msec depolarizations to various test potentials (−80 mV to 20 mV) from a holding potential of −120 mV. Sodium conductance (g_{Na}) was calculated according to the equation $g_{Na} = I_{Na}/(V_g - V_r)$, where I_{Na} is the peak amplitude of the Na^+ current, V_g is the test potential, and V_r is the reversal potential for Na^+. To compare voltage dependence of activation, data were fitted by the least-squares fit of the data to a Boltzmann function, according to the equation $g_{Na}/g_{Namax} = 1 - 1/\{1 - \exp[(V_h - V_{1/2})/k]\}$, where g_{Namax} is the maximum conductance, V_h is the potential of individual step pulses, $V_{1/2}$ is the potential at which g_{Na} is one-half maximal, and k is the slope factor. The data points represent the average of g_{Na}/g_{Namax}. Note that E1211K and I1473M opened at significantly lower voltages. (B) Half activation potentials of $Na_v1.2$ channels. Half activation potentials were calculated for individual cells and averaged. (C) Steady-state voltage dependence of inactivation for WT (closed circle), E1211K (closed triangle), I1473M (open triangle), and A575V (open circle). Cells were pre-pulsed for 2 seconds at various holding potentials (from −120 mV to 10 mV in 10-mV increments), and then Na^+ current was evoked by a step depolarization to 0 mV. The peak amplitudes of the Na^+ currents measured at individual test potentials were normalized to the peak amplitude of the Na^+ current measured at a holding potential of −120 mV. Data were fitted by the least-squares fit of the data to a Boltzmann function, according to the equation $I/I_{max} = 1/\{1 + \exp[(V_h - V_{1/2})/k]\}$, where I_{max} is the magnitude of the peak Na^+ current observed at a holding potential of −120 mV, V_h is the holding potential, $V_{1/2}$ is the potential at which the Na^+ current is one-half maximal, and k is the slope factor. The data points represent the average of I/I_{max}. Note that the curve for E1211K is significantly shifted to the hyperpolarized direction. (D) Half inactivation potentials of $Na_v1.2$ channels. Half inactivation potentials were calculated for individual cells and averaged. Values represent means ± SEM, $^*p < 0.05$, $^{**}p < 0.01$.

and invertebrate VGSC α subunits and human voltage-gated calcium channel α subunits (figure 2). Similarly, the isoleucine residue of *SCN2A*-I1473M putatively located on S6 of DIII was perfectly conserved through vertebrate and invertebrate VGSC α subunits. These conserved amino acids implicated a pathogenic potential for E1211K and I1473M.

The alanine residue of *SCN2A*-A575V putatively located at the intracellular linker connecting DI and DII was conserved in human, mice, and rat $Na_v1.2$, but not in other human VGSC α subunits (figure 2).

E1211K and I1473M mutant channels exhibit significantly altered electrophysiologic properties. To investigate the functional consequences of *SCN2A*-E1211K, I1473M, and A575V, we examined the electrophysiologic properties of the human wild-type (WT) and mutant (E1211K, I1473M, and A575V) $Na_v1.2$ expressed heterologously in HEK293 cells in the presence of human VGSC β_I and β_{II} subunits using whole-cell patch-clamp recordings. Western blot analysis showed no differences in protein expression levels among WT, E1211K, I1473M, and A575V (figure e-2 and e-Methods).

Half-activation potentials in E1211K and I1473M were significantly shifted to the hyperpolarized direction relative to WT ($p = 0.001$ and 0.004); in contrast, A575V displayed values similar to WT (figure 3, A and B). Average half activation potentials calculated from the pooled data were −17.1 ± 3.8 mV (n = 12) for WT, −35.2 ± 3.5 mV (n = 12) for E1211K, −31.3 ± 3.0 mV (n = 15) for I1473M, and −19.9 ± 2.9 mV (n = 8) for A575V.

Next, we examined the steady-state voltage dependence of inactivation. Half-inactivation potentials in E1211K displayed a significant shift to the hyperpolarized direction compared to WT ($p = 0.0001$) (figure 3, C and D). Average half inactivation potentials calculated from the pooled data were −64.8 ± 4.7 mV (n = 11) for WT, −86.9 ± 2.2 mV (n = 12) for E1211K, −59.5 ± 1.9 mV (n = 13) for I1473M, and −70.1 ± 2.6 mV (n = 7) for A575V.

We then investigated the time course of recovery from the inactivated state using a double pulse protocol. E1211K showed a pronounced delay of recovery from inactivation compared to WT ($p = 0.02$), whereas I1473M and A575V exhibited time courses similar to WT (figure 4A). Average of A_{rec} calculated from the pooled data were 0.58 ± 0.12 (n = 11) for WT, 0.30 ± 0.03 (n = 12) for E1211K, 0.78 ± 0.12 (n = 15) for I1473M, and 0.53 ± 0.09 (n = 8) for A575V (figure 4B).

Taken altogether, E1211K and I1473M markedly altered the voltage-dependence of $Na_v1.2$, indicating high pathogenic potentials of E1211K and

Figure 4 Recovery from inactivated state for human wild-type and mutant (E1211K, I1473M, and A575V) $Na_v1.2$ channels

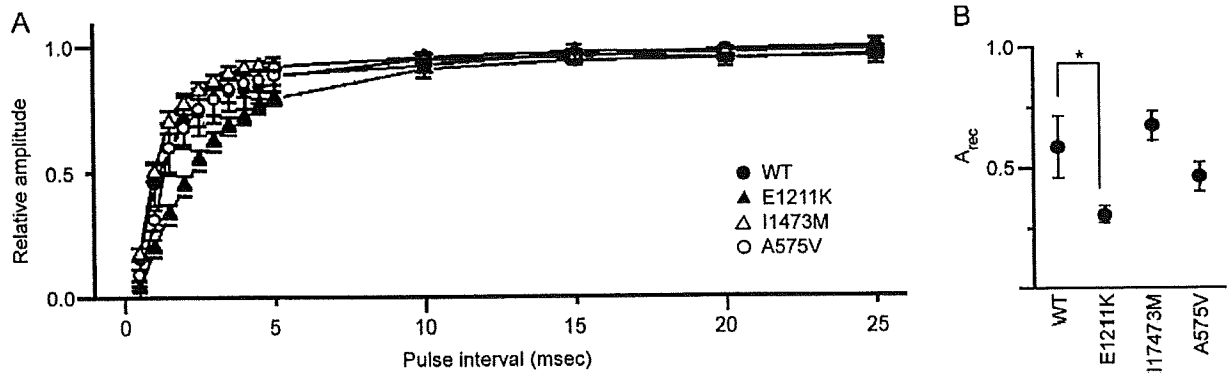

(A) Recovery from inactivated state for WT (closed circle), E1211K (closed triangle), I1473M (open triangle), and A575V (open circle). Two depolarizing pulses (step to 10 mV, 10 msec in duration) with various interpulse intervals (from 0.5 msec to 50 msec) were successively applied to activate Na^+ currents. The peak amplitude of Na^+ currents evoked by the second pulse (I_2) was normalized to the peak amplitude of Na^+ currents evoked by the first pulse (I_1) and I_2/I_1 is expressed as recovery ratios. Data were fitted by the equation $I_2/I_1 = 1 - \exp(-A_{rec}t)$, where A_{rec} is the factor to determine the speed of recovery. The data points represent the average of I_2/I_1. Note that the recovery for E1211K was significantly prolonged. (B) A_{rec} of $Na_v1.2$ channels. A_{rec} was calculated for individual cells and averaged. Values represent means ± SEM, $^*p < 0.05$, $^{**}p < 0.01$.

I1473M. In contrast, A575V caused no significant effects on the voltage dependence of $Na_v1.2$, suggesting low pathogenicity of A575V.

DISCUSSION We identified 2 plausible pathogenic de novo *SCN2A* mutations, E1211K and I1473M, in 2 sporadic intractable childhood epilepsy cases. Together with the de novo R102X,[18] which we previously discovered in a patient with sporadic intractable childhood epilepsy, these mutations indicate that *SCN2A* is a plausible etiologic candidate gene underlying intractable childhood epilepsies.

One de novo mutation, E1211K, was identified in a patient with sporadic infantile spasms that progressed into severe symptomatic generalized epilepsy. Although the patient was born with mild asphyxia, we surmise that it would be insufficient to cause the sporadic infantile spasms and favor the notion that the de novo E1211K is the most possible primary cause. A respiratory arrest caused by a status epilepticus at age 17 years plausibly accounts for the rapid deterioration of his physical and mental condition.

The electrophysiologic analyses revealed that E1211K significantly altered the functional properties of $Na_v1.2$ channel. E1211K caused a large hyperpolarizing shift of the voltage dependence of activation, affecting a reduction in the threshold of depolarization required for activation. E1211K also caused the left shift of the voltage dependence of steady-state inactivation, suggesting that, at the physiologic resting membrane potential (−70 to −60 mV), more than 85% of $Na_v1.2$ carrying E1211K would be in the inactivated state in comparison to ~50% wild-type $Na_v1.2$. Furthermore, E1211K delayed the recovery from inactivated state possibly leading to a reduction in channel availability during repetitive firings. Taken altogether, E1211K produced mutant channels with mixed electrophysiologic properties indicating both augmented and reduced channel activities. Overall, the effects of E1211K on the excitability of neurons are currently difficult to predict. The consequences on the ultimate neuronal excitability might depend on other cellular conditions and the localization in specific neuronal types.

The other de novo mutation, I1473M, was identified in a patient with unusual neonatal epileptic encephalopathy.[19] $Na_v1.2$ channel carrying I1473M showed a significant shift of the voltage dependence of activation to the hyperpolarized direction, suggesting that this mutation may increase the channel activity and thereby may cause hyperexcitation of neurons leading to epileptic seizures. Epileptic seizures responded to lidocaine, which might possibly reduce VGSC activities by affecting not only the mutant $Na_v1.2$ channel but also wild-type $Na_v1.2$ and other brain-type VGSCs.

We also identified an inherited mutation, A575V, in a patient with SMEB, which was not observed in our 311 healthy control individuals. Given that A575V was found in her asymptomatic father and that the functional effect of A575V on human $Na_v1.2$ was insignificant, A575V is most likely a rare nonpathogenic variant. However, it could be also possible that A575V contributes to the susceptibility to develop epileptic seizures when combined with additional genetic or environmental modifiers, present in the patient but not in the father.

This and our previous studies have provided a total of 3 de novo *SCN2A* mutations: E1211K, I1473M,

and R102X.[18] Notably, these mutations associated with distinct epileptic phenotypes and affected channel properties of $Na_v1.2$ differentially. There are 2 possible explanations for the phenotypic varieties. First, phenotypic variability could be due to the individual mutation or its location in the $Na_v1.2$ protein, which could differentially affect protein stability, subcellular trafficking, or channel functions. Alternatively, *SCN2A* mutation mosaicism might be related to phenotypic variations. When de novo mutations occur during early development, the patients could be somatic mosaics for their mutations, and therefore brain regions in those patients could be affected differentially, leading to phenotypic variability. In support of this idea, *SCN1A* mutation mosaicism occurs in some mildly affected or asymptomatic patients' parents in several familial SMEI cases.[20-23]

Of *SCN2A* mutations identified in BFNIS patients so far,[14-17] 4 were studied using patch-clamp recordings and had $Na_v1.2$ channels with altered channel properties predicting a gain of function[24,25] or with reduced cell surface expression implicating a loss of function.[26] Although there was a discrepancy among the results, the amounts of changes in half activation and half inactivation potentials by the BFNIS mutations were within ±6 mV. By contrast, the amounts of changes in half activation and half inactivation potentials in *SCN2A*-E1211K were ~−18-mV and ~−22-mV, and that of the half activation potential in *SCN2A*-I1473M was ~−14-mV. Thus, both E1211K and I1473M altered the channel properties of $Na_v1.2$ to a greater extent than the BFNIS mutations, suggesting a mechanism for more severe epileptic phenotypes. In order to confirm these correlations, the effects of the mutations on the functions of the neurons responsible for seizure development, which are currently unknown, should be examined further.

SCN1A mutant mice with spontaneous epileptic seizures have reduced *SCN1A* expression.[27,28] Further, *SCN1A* is prominently expressed in the parvalbumin-positive inhibitory interneurons and we proposed that *SCN1A* mutations might cause functional defects in the parvalbumin-positive interneurons, which then fail to suppress overexcitation of neural circuits and result in epileptic seizures.[28] In contrast to the case for *SCN1A* mutations, the molecular mechanisms underlying seizures caused by *SCN2A* mutations remain largely unknown. Since *SCN2A* is highly expressed in both principal neurons and interneurons in rat hippocampus,[29,30] *SCN2A* mutations might alter the global function of the implicated neurons. Although loss or reduced *SCN2A* expression did not generate spontaneous epileptic seizures in mice,[31] our present study and others' provide solid genetic evidence implicating *SCN2A* in the etiology of human epilepsies.[14-18] Further studies using mouse models with the *SCN2A* mutations identified in human epilepsies may help to understand the impact of such mutations on the epileptic brain.

AUTHOR CONTRIBUTIONS

Statistical analysis was conducted by Dr. M. Kaneda.

ACKNOWLEDGMENT

The authors thank all the patients and families for their contributions and cooperation. They also thank Drs. Oyama and Nukina (RIKEN Brain Science Institute) for rabbit anti-VGSC β_1 antibody, Drs. Kaneko (Hirosaki University) and Hirose (Fukuoka University) for providing materials, Ms. Shibazaki for laboratory support, and Research Resource Center of RIKEN Brain Science Institute for DNA sequencing and genotyping analyses.

Received February 25, 2009. Accepted in final form June 18, 2009.

REFERENCES

1. Meisler MH, Kearney JA. Sodium channel mutations in epilepsy and other neurological disorders. J Clin Invest 2005;115:2010–2017.
2. Mulley JC, Scheffer IE, Petrou S, Dibbens LM, Berkovic SF, Harkin LA. SCN1A mutations and epilepsy. Hum Mutat 2005;25:535–542.
3. Escayg A, MacDonald BT, Meisler MH, et al. Mutations of *SCN1A*, encoding a neuronal sodium channel, in two families with GEFS+2. Nat Genet 2000;24:343–345.
4. Sugawara T, Mazaki-Miyazaki E, Ito M, et al. Nav1.1 mutations cause febrile seizures associated with afebrile partial seizures. Neurology 2001;57:703–705.
5. Claes L, Del-Favero J, Ceulemans B, Lagae L, Van Broeckhoven C, De Jonghe P. De novo mutations in the sodium-channel gene *SCN1A* cause severe myoclonic epilepsy of infancy. Am J Hum Genet 2001;68:1327–1332.
6. Sugawara T, Mazaki-Miyazaki E, Fukushima K, et al. Frequent mutations of SCN1A in severe myoclonic epilepsy in infancy. Neurology 2002;58:1122–1124.
7. Fujiwara T, Sugawara T, Mazaki-Miyazaki E, et al. Mutations of sodium channel α subunit type 1 (SCN1A) in intractable childhood epilepsies with frequent generalized tonic-clonic seizures. Brain 2003;126:531–546.
8. Fukuma G, Oguni H, Shirasaka Y, et al. Mutations of neuronal voltage-gated Na^+ channel α1 subunit gene *SCN1A* in core severe myoclonic epilepsy in infancy (SMEI) and in borderline SMEI (SMEB). Epilepsia 2004;45:140–148.
9. Scheffer IE, Berkovic SF. Generalized epilepsy with febrile seizures plus: a genetic disorder with heterogeneous clinical phenotypes Brain 1997;120:479–490.
10. Dravet C, Bureau M, Oguni H, Fukuyama Y, Cokar O. Severe myoclonic epilepsy in infancy (Dravet syndrome). In: Roger J, Bureau M, Dravet C, Genton P, Tassinari CA, Wolf P, eds. Epileptic Syndromes in Infancy, Childhood and Adolescence, 4th ed. Montrouge, France: John Libbey Eurotext; 2005:89–113.
11. Wallace RH, Hodgson BL, Grinton BE, et al. Sodium channel α1-subunit mutations in severe myoclonic epilepsy of infancy and infantile spasms. Neurology 2003;61:765–769.
12. Harkin LA, McMahon JM, Iona X, et al. The spectrum of *SCN1A*-related infantile epileptic encephalopathies. Brain 2007;130:843–852.
13. Sugawara T, Tsurubuchi Y, Agarwala KL, et al. A missense mutation of the Na^+ channel α_{II} subunit gene *$Na_v1.2$* in a

patient with febrile and afebrile seizures causes channel dysfunction. Proc Natl Acad Sci USA 2001;98:6384–6389.
14. Berkovic SF, Heron SE, Giordano L, et al. Benign familial neonatal-infantile seizures: characterization of a new sodium channelopathy. Ann Neurol 2004;55:550–557.
15. Heron SE, Crossland KM, Andermann E, et al. Sodium-channel defects in benign familial neonatal-infantile seizures. Lancet 2002;360:851–852.
16. Striano P, Bordo L, Lispi ML, et al. A novel *SCN2A* mutation in family with benign familial infantile seizures. Epilepsia 2006;47:218–220.
17. Herlenius E, Heron SE, Grinton BE, et al. SCN2A mutations and benign familial neonatal-infantile seizures: the phenotypic spectrum. Epilepsia 2007;48:1138–1142.
18. Kamiya K, Kaneda M, Sugawara T, et al. A nonsense mutation of the sodium channel gene *SCN2A* in a patient with intractable epilepsy and mental decline. J Neurosci 2004;24:2690–2698.
19. Sawaishi Y, Yano T, Enoki M, Takada G. Lidocaine-dependent early infantile status epilepticus with highly suppressed EEG. Epilepsia 2002;43:201–204.
20. Depienne C, Arzimanoglou A, Trouillard O, et al. Parental mosaicism can cause recurrent transmission of *SCN1A* mutations associated with severe myoclonic epilepsy of infancy. Hum Mutat 2006;27:389.
21. Gennaro E, Santorelli FM, Bertini E, et al. Somatic and germline mosaicisms in severe myoclonic epilepsy of infancy. Biochem Biophys Res Commun 2006;341:489–493.
22. Marini C, Mei D, Helen Cross J, Guerrini R. Mosaic *SCN1A* mutation in familial severe myoclonic epilepsy of infancy. Epilepsia 2006;47:1737–1740.
23. Morimoto M, Mazaki E, Nishimura A, et al. SCN1A mutation mosaicism in a family with severe myoclonic epilepsy in infancy. Epilepsia 2006;47:1732–1736.
24. Scalmani P, Rusconi R, Armatura E, et al. Effects in neocortical neurons of mutations of the $Na_v1.2$ Na^+ channel causing benign familial neonatal-infantile seizures. J Neurosci 2006;26:10100–10109.
25. Xu R, Thomas EA, Jenkins M, et al. A childhood epilepsy mutation reveals a role for developmentally regulated splicing of a sodium channel. Mol Cell Neurosci 2007;35:292–301.
26. Misra SN, Kahlig KM, George AL, Jr. Impaired $Na_V1.2$ function and reduced cell surface expression in benign familial neonatal-infantile seizures. Epilepsia 2008;49:1535–1545.
27. Yu FH, Mantegazza M, Westenbroek RE, et al. Reduced sodium current in GABAergic interneurons in a mouse model of severe myoclonic epilepsy in infancy. Nat Neurosci 2006;9:1142–1149.
28. Ogiwara I, Miyamoto H, Morita N, et al. $Na_v1.1$ localizes to axons of parvalbumin-positive inhibitory interneurons: a circuit basis for epileptic seizures in mice carrying an *Scn1a* gene mutation. J Neurosci 2007;27:5903–5914.
29. Furuyama T, Morita Y, Inagaki S, Takagi H. Distribution of I, II and III subtypes of voltage-sensitive Na^+ channel mRNA in the rat brain. Brain Res Mol Brain Res 1993;17:169–173.
30. Black JA, Yokoyama S, Higashida H, Ransom BR, Waxman SG. Sodium channel mRNAs I, II and III in the CNS: cell-specific expression Brain Res Mol Brain Res 1994;22:275–289.
31. Planells-Cases R, Caprini M, Zhang J, et al. Neuronal death and perinatal lethality in voltage-gated sodium channel α_{II}-deficient mice. Biophys J 2000;78:2878–2891.

ARTICLE IN PRESS

ELSEVIER

Brain & Development xxx (2009) xxx–xxx

BRAIN & DEVELOPMENT
Official Journal of the Japanese Society of Child Neurology

www.elsevier.com/locate/braindev

Case report

Mild phenotype in Pelizaeus-Merzbacher disease caused by a *PLP1*-specific mutation

Hitoshi Osaka [a,e,*], Shiro Koizume [a,e], Haruhiko Aoyama [d], Hiroko Iwamoto [d], Seiji Kimura [d], Jun-ichi Nagai [b], Kenji Kurosawa [c], Sumimasa Yamashita [a]

[a] *Division of Neurology, Clinical Research Institute, Kanagawa Children's Medical Center, Yokohama 232-855, Japan*
[b] *Division of Laboratory Medicine, Clinical Research Institute, Kanagawa Children's Medical Center, Yokohama 232-855, Japan*
[c] *Division of Genetics, Clinical Research Institute, Kanagawa Children's Medical Center, Yokohama 232-855, Japan*
[d] *Division of Pediatric Neurology, Yokohama Ryoiku-iryo Center, Yokohama 241-0014, Japan*
[e] *Molecular Pathology & Genetics Division, Kanagawa Cancer Center Research Institute, Yokohama 241-0815, Japan*

Received 7 May 2009; received in revised form 1 November 2009; accepted 6 November 2009

Abstract

We present the case of a 26 year-old man who developed normally until he began having difficulty walking at age 12. He subsequently became unable to stand at 15 years old and exhibited mental regression and generalized tonic convulsions by age 20. Magnetic resonance imaging revealed incomplete myelination of cerebral white matter, which resembled that of Pelizaeus-Merzbacher disease. By sequencing the proteolipid protein 1 (*PLP1*) gene, we found a novel mutation (c.352_353delAG (p.Gly130fs)) in the latter half of exon 3 (exon 3B) that is spliced out in the DM20 isoform. Exon 3B mutations are known to cause a mild phenotype since they do not disturb DM20 production. Mutations that truncate PLP1 correlate with a mild phenotype by activating the nonsense-mediated decay mechanism that specifically detects and degrades mRNAs containing a premature termination codon. This attenuates the production of toxic mutant PLP1. The very mild presentation in the present case seems to be derived from the unique nature of the mutation, which preserves DM20 production and decreases mutant PLP1.

Keywords: Pelizaeus-Merzbacher disease; Proteolipid protein 1; *PLP1*

1. Introduction

Proteolipid protein (PLP) 1 and its splice isoform DM20 are encoded by the *PLP1* gene. PLP1/DM20 proteins are major components of myelin expressed in oligodendrocytes in central nervous system (CNS) [1]. PLP1/DM20 translated in the endoplasmic reticulum (ER) is transported to the cell surface and integrated into plasma membrane presumably via four membrane-spanning domains with both amino- and carboxy-terminal ends on cytoplasmic side. Owing to its strong hydrophobicity, PLP1/DM20 can form a stable compact myelin sheath in cooperation with other myelin proteins [1]. Expression of PLP1 and DM20 are spatially and temporally regulated. DM20 expresses preferentially in embryonic stages in a variety of cell types, whereas PLP1 expresses postnatally in oligodendrocytes. Both PLP1 and DM20 constitute the predominant protein in myelin [2].

Pelizaeus-Merzbacher disease (PMD) is a severe X-linked recessive disorder caused by mutations of the *PLP1* gene [1]. A deficiency in PLP1/DM20 at the cell

* Corresponding author. Address: Division of Neurology, Clinical Research Institute, Kanagawa Children's Medical Center, Mutsukawa 2-138-4, Minami-ku, Yokohama 232-8555, Japan. Tel.: +81 45 711 2351; fax: +81 45 721 332.
E-mail address: hosaka@kcmc.jp (H. Osaka).

0387-7604/$ - see front matter © 2009 Elsevier B.V. All rights reserved.
doi:10.1016/j.braindev.2009.11.004

Please cite this article in press as: Osaka H et al. Mild phenotype in Pelizaeus-Merzbacher disease caused by a *PLP1*-specific mutation. Brain Dev (2009), doi:10.1016/j.braindev.2009.11.004

membrane by PLP1 mutation leads to the arrest of myelination. Moreover, mutant PLP1 elicits a response in the ER, which attempt to refold the misfolded mutant PLP1/DM 20 protein [3]. However, if the level of misfolded protein exceeds the controllable limit within the ER quality control system, apoptotic signals are transduced from ER [3]. This cellular process is reflected in developmental regression and atrophy of the CNS.

Exonic or intron/exon boundary mutations are found in 20–30% of PMD patients and phenotypes are severer than other mutations such as total deletion and duplication of *PLP1*. An exception has been observed in the latter half of exon 3 (exon 3B) of *PLP1* [4–8]. Mutations within this region are predicted not to disturb DM20 expression and function. Mutations that truncate PLP1 are related to a mild phenotype presumably by activating the nonsense-mediated decay (NMD) pathway, a mechanism that specifically detects and degrades mRNAs containing a premature termination codon [9]. This attenuates the production of mutant PLP1 levels and thus likely lessens the ER stress responses. In this report, we present a PMD patient with a very mild phenotype. We identified a novel *PLP1* gene mutation that is predicted to preserve DM20 production and results in a frame-shifted mutant PLP1 protein.

2. Materials and methods

2.1. Patient

This 26 year-old boy was born uneventfully at full term to Japanese parents. He was born with a body weight of 3660 g and an Apgar score of 9/9 at 1 and 5 min. No stridor or nystagmus was noted. He gained head control at 4 months, could sit without support at 8 months, and could walk without assistance at 4 years. He was pointed out spasticity of lower limbs and EEG abnormalities at 1 year. He was treated with carbamazepine for 14 years. No seizures occurred during that period. He could speak a few words at 2 years of age. He attended a special class in normal elementary and junior high school. He had no difficulties in daily conversation and writings. The patient began having difficulty walking at 12 years of age and became unable to stand at 15 years. He showed frequent urination and was diagnosed as neurogenic bladder at 15 years. MRI taken at that time revealed only mild ventricular enlargement. Myelination was not evaluated because of the motion artifact. At age 20, he showed signs of mental regression and began speaking fewer words. He exhibited generalized tonic convulsions and was treated with valproic acid at 24 years. He was subsequently referred to a hospital for evaluation. He was not small for his ages with a height of 167 cm and a weight of 54 kg. He could conversate with combining two words. He showed no nystagmus and exhibited alternating outer-nystagmus and oculomoter apraxia. He could walk with assistance. His muscle tone was hypertonic in the upper limbs. Clumsiness was observed with all extremities displaying exaggerated tendon reflexes and bilateral extensor plantar responses. Speech was slurred and dysmetry with terminal oscillation and dysdiadochokinesis were observed. Routine laboratory examinations revealed no biochemical abnormalities in the level of serum ammonia, lactate and pyruvate, very long chain fatty acids, or arylsulfatase A. Nerve conduction velocities and electromyographic studies were all normal. Measurement of auditory evoked brain responses revealed only wave I. MRI revealed a completion of myelination in the T1 signal. Myelination in the white matter was incomplete in the T2 signal (Fig. 1).

2.2. Genomic DNA sequencing

Genomic DNA from this patient was prepared from white blood cells using the Wizard Genomic DNA puri-

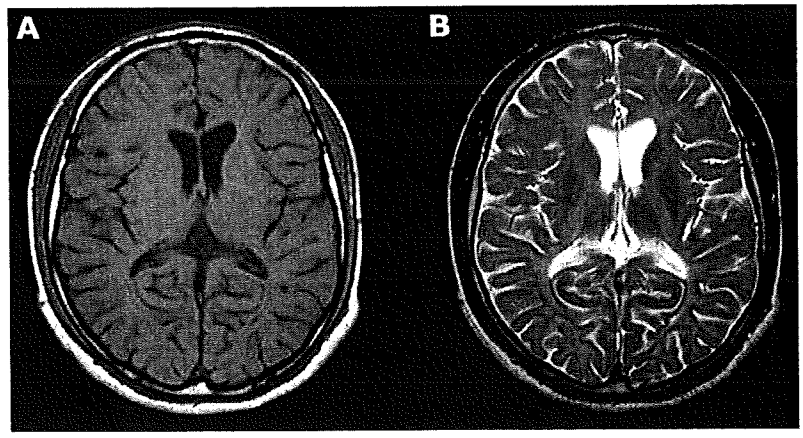

Fig. 1. Magnetic resonance imaging (MRI) at 26 year-old patient shows disappearance of contrast between cortex and white matter (A) on a T1-weighted image. T2-weighted image shows the incompletion of myelination in the white matter (B).

Please cite this article in press as: Osaka H et al. Mild phenotype in Pelizaeus-Merzbacher disease caused by a *PLP1*-specific mutation. Brain Dev (2009), doi:10.1016/j.braindev.2009.11.004

fication kit (Promega, Madison, WI USA). PCR of seven exons and promoter regions of the *PLP1* gene was performed as previously described [10]. Subsequent sequencing analyses of the PCR fragments were performed by direct sequencing using the Big Dye Terminators v1.1 Cycle Sequencing kit (Applied Biosystems Foster City, CA). Duplication was screened by FISH as described [10].

3. Results

By direct sequencing of the patient's *PLP1* gene exons, exon/intron boundaries and a promoter region, we found a novel mutation in exon 3: c.352_353delAG (p.Gly130fs) (Fig. 2). No other sequence alterations were found and this mutation was not detected in more than 200 alleles. This two nucleotide deletion occurs in the latter half of exon 3 (exon 3B), which is not involved in *DM20* mRNA production (Fig. 3). FISH analysis showed normal copy numbers in this patient.

4. Discussion

Pelizaeus-Merzbacher disease belongs to leukodystrophies, one of a group of disorders that affect the white matter of the CNS. Genetic defects in PLP1/DM20, the most predominant myelin proteins, causes dual pathology: defects in CNS myelin formation (dysmyelination)

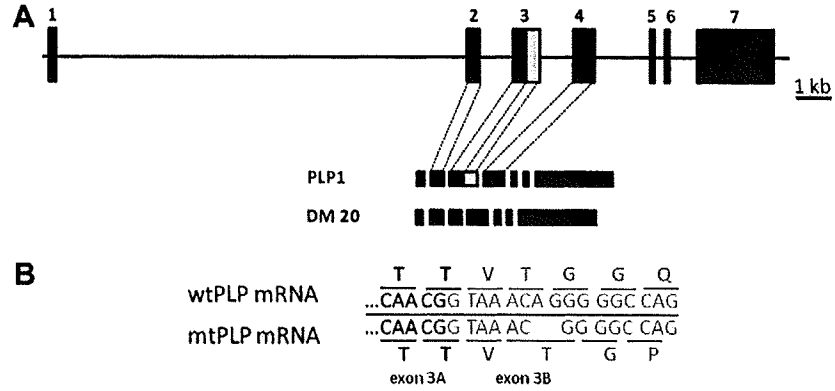

Fig. 2. Splicing the *PLP1* gene into *PLP1* mRNA and *DM20* mRNA. (A) Schematic presentation of *PLP1* gene structure. (upper panel) PLP1 gene is composed of seven exons. (lower panel) mRNA of PLP1/DM20 differs in only the latter half of exon 3 that is spliced out for the production of DM20 mRNA. (B) Two nucleotide deletion and subsequent frame shift in the Patient. Novel mutation in exon 3B, c.352_353delAG (p.Gly130fs), causes the frame shift in *PLP1* mRNA.

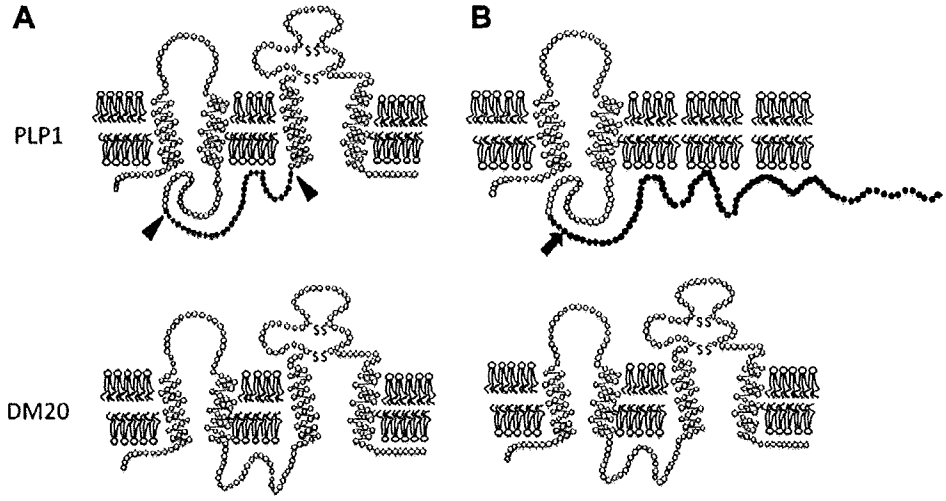

Fig. 3. Deduced PLP1 gene products; PLP1 and DM20. (A) Wild-type PLP1 (upper) and DM20 (lower) which are thought to include 4 membrane-spanning domains. Thirty-five intracellular amino acids (gray circle; between arrow head) are lacking in DM20. One circle corresponds to one amino acid. (B) PLP1 and DM20 of the patient. (upper) A two nucleotides deletion in exon 3B, c.352_353delAG (p.Gly130fs), causes a frame shift (arrow) and extension that are composed of 82 nonsense peptides. (lower) DM20 is identical to wild-type in this patient.

Please cite this article in press as: Osaka H et al. Mild phenotype in Pelizaeus-Merzbacher disease caused by a *PLP1*-specific mutation. Brain Dev (2009), doi:10.1016/j.braindev.2009.11.004

and oligodendrocytes cell loss via apoptosis. PLP1 and DM20 are required for myelin compaction. Mutations in the *PLP1* gene, such as total deletion and truncation mutations, cause an inability to form normal myelin, which is easily revealed by diffuse high signals in all CNS white matter in T2-weighted MRI scans. Since PLP1/DM20 are constitute more than 50% of the protein in oligodendrocytes, mutant PLP1/DM20 cause the excessive ER stress responses and subsequent cell death that can be visualized by MRI/CT as brain atrophy.

Typically, patients with PMD show neonatal nystagmus and developmental delay that becomes apparent during infancy. Impairments of motor functions involve spastic paresis from the defect in the corticospinal tract, intention tremor from abnormalities in the cerebellar pathway, and choreoathetosis and rigidity due to basal ganglia dysfunction. Although all patients exhibit mental retardation, psycho-intellectual development is greater than motor development. Lesions are restricted in the myelinated portion in the CNS but disease severity varies considerably.

Cailloux et al. graded the clinical severity of PMD patients by their maximal motor achievements. Patients with Form 0 never gain head control ability, whereas patients with Form 1 can achieve head control. Form 2 includes the patients who are able to maintain a sitting position. Form 3 includes patients who can walk with support, while patients with Form 4 can walk autonomously. This last form overlaps the clinical phenotype of X-linked spastic paraplegia type 2, the allelic disease to PMD [8]. The patient described in the present case report belongs to Form 4, the mildest symptom group.

Amino acid substitutions, especially conserved amino acids in DM20/PLP1 within species, usually cause a severe phenotype [6]. Duplication of PLP1 causes a milder form, in which patients gain head control or sitting ability. Two types of mutations cause the mildest form of PMD. One type is total gene deletion, a truncation mutation that does not cause the mutant PLP1 that elicit the ER stress responses, and the second is the *PLP1*-specific exon 3B mutation.

Here, we described a patient with a mild form of PMD who could speak meaningful words and walk independently until 15 years of ages. He had two nucleotide deletions within exon 3B which are spliced out during *DM20* messenger RNA production. This mutation preserves the expression and function of DM20 protein. Moreover, this mutant protein is much shorter than wild-type PLP (277/241aa). It should easily be degraded via the activation of nonsense-mediated decay (NMD) pathway, a mechanism that specifically detects and degrades mRNAs containing a premature termination codon. The very mild phenotype observed is probably due to the dual effect of mutation: conservation of DM20 and the inability to elicit an ER stress response.

Thirteen different mutations have been reported in exon 3B (c.384C>G, 385C>T, 388C>T, 409C>G, 409C>T, 410delG, 418C>T, 430A>T, 434G>A, 441A>T, 442C>T, 446C>T). Twelve of them are one nucleotide changes and are predicted to preserve DM20 expressions. Clinical presentations are reported in 9 cases and 6 fit the criteria of Form 4, reinforcing the importance of DM20 function in addition to PLP1. Thus far, only one example of an exon 3B mutation that causes normal DM20 and truncated PLP1 has been reported (440delG; R137fsX8) [6]. This mutation caused two patients with Form 3 and one with Form 4. Our case is the second examples of an exon 3B mutation that produce normal DM20 and truncational PLP1. Our case, together with reports of other exon 3B mutations, supports the hypothesis that frame-shift mutations of PLP1 in exon 3B underlies the very mild phenotype in PMD.

Acknowledgements

We thank Mariko Kitajima for technical assistance. This work was supported in part by Grants-in-Aid from Scientific Research from the Ministry of Health, Labor and Welfare of Japan, Health and Labor Science Research Grant of Japan, Yokohama Foundation for Advancement of Medical Science, Takeda Science Foundation and Kanagawa Municipal Hospital Pediatric Research.

References

[1] Inoue K. PLP1-related inherited dysmyelinating disorders: Pelizaeus-Merzbacher disease and spastic paraplegia type 2. Neurogenetics 2005;6:1–16.

[2] Taylor CM, Marta CB, Claycomb RJ, Han DK, Rasband MN, Coetzee T, et al. Proteomic mapping provides powerful insights into functional myelin biology. Proc Natl Acad Sci USA 2004;101:4643–8, [in English].

[3] Southwood CM, Garbern J, Jiang W, Gow A. The unfolded protein response modulates disease severity in Pelizaeus-Merzbacher disease. Neuron 2002;36:585–96.

[4] Hubner CA, Orth U, Senning A, Steglich C, Kohlschutter A, Korinthenberg R, et al. Seventeen novel PLP1 mutations in patients with Pelizaeus-Merzbacher disease. Hum Mutat 2005;25:321–2.

[5] Nance MA, Boyadjiev S, Pratt VM, Taylor S, Hodes ME, Dlouhy SR. Adult-onset neurodegenerative disorder due to proteolipid protein gene mutation in the mother of a man with Pelizaeus-Merzbacher disease. Neurology 1996;47:1333–5.

[6] Hobson GM, Huang Z, Sperle K, Sistermans E, Rogan PK, Garbern JY, et al. Splice-site contribution in alternative splicing of PLP1 and DM20: molecular studies in oligodendrocytes. Hum Mutat 2006;27:69–77.

[7] Cailloux F, Gauthier-Barichard F, Mimault C, Isabelle V, Courtois V, Giraud G, et al. Genotype–phenotype correlation in inherited brain myelination defects due to proteolipid protein gene mutations. Clinical European Network on Brain Dysmyelinating Disease. Eur J Hum Genet 2000;8:837–45.

Please cite this article in press as: Osaka H et al. Mild phenotype in Pelizaeus-Merzbacher disease caused by a *PLP1*-specific mutation. Brain Dev (2009), doi:10.1016/j.braindev.2009.11.004

[8] Osaka H, Kawanishi C, Inoue K, Uesugi H, Hiroshi K, Nishiyama K, et al. Novel nonsense proteolipid protein gene mutation as a cause of X-linked spastic paraplegia in twin males. Biochem Biophys Res Commun 1995;215:835–41.

[9] Inoue K, Khajavi M, Ohyama T, Hirabayashi S, Wilson J, Reggin JD, et al. Molecular mechanism for distinct neurological phenotypes conveyed by allelic truncating mutations. Nat Genet 2004;36:361–9.

[10] Osaka H, Kawanishi C, Inoue K, Onishi H, Kobayashi T, Sugiyama N, et al. Pelizaeus-Merzbacher disease: three novel mutations and implication for locus heterogeneity. Ann Neurol 1999;45:59–64.

Please cite this article in press as: Osaka H et al. Mild phenotype in Pelizaeus-Merzbacher disease caused by a *PLP1*-specific mutation. Brain Dev (2009), doi:10.1016/j.braindev.2009.11.004

J Inherit Metab Dis
DOI 10.1007/s10545-009-9022-9

RAPID COMMUNICATION

A new case of GABA transaminase deficiency facilitated by proton MR spectroscopy

Megumi Tsuji · Noriko Aida · Takayuki Obata · Moyoko Tomiyasu · Noritaka Furuya · Kenji Kurosawa · Abdellatif Errami · K. Michael Gibson · Gajja S. Salomons · Cornelis Jakobs · Hitoshi Osaka

Received: 2 October 2009 / Revised: 29 October 2009 / Accepted: 23 November 2009

Abstract
Background Deficiency of 4-aminobutyrate aminotransferase (GABA-T) is a rare disorder of GABA catabolism, with only a single sibship reported. We report on a third case, a Japanese female infant with severe psychomotor retardation and recurrent episodic lethargy with intractable seizures, with the diagnosis facilitated by proton magnetic resonance (MR) spectroscopy (^{1}H-MRS).
Methods Neuroimaging was performed at the first episode of lethargy. For ^{1}H-MRS, locations were placed in the semioval center and the basal ganglia. Quantification of metabolite concentrations were derived using the LCModel. We confirmed the diagnosis subsequently by enzyme and molecular studies, which involved direct DNA sequence analysis and the development of a novel multiplex ligation-dependent probe amplification test.
Results ^{1}H-MRS analysis revealed an elevated GABA concentration in the basal ganglia (2.9 mmol/l). Based on the results of quantitative ^{1}H-MRS and clinical findings, GABA-T deficiency was suspected and confirmed in cultured lymphoblasts. Molecular studies of the *GABA-T* gene revealed compound heterozygosity for a deletion of one exon and a missense mutation, 275G>A, which was not detected in 210 control chromosomes.
Conclusions Our results suggest that excessive prenatal GABA exposure in the central nervous system (CNS) was responsible for the clinical manifestations of GABA transaminase deficiency. Our findings suggest the dual

Communicated by: Marinus Duran

M. Tsuji · H. Osaka (✉)
Division of Neurology, Clinical Research Institute,
Kanagawa Children's Medical Center,
2-138-4 Mutsukawa, Minami-ku,
Yokohama 232-8555, Japan
e-mail: hosaka@kcmc.jp

N. Aida
Division of Radiology, Clinical Research Institute,
Kanagawa Children's Medical Center,
2-138-4 Mutsukawa, Minami-ku,
Yokohama 232-8555, Japan

N. Furuya · K. Kurosawa
Division of Genetics, Clinical Research Institute,
Kanagawa Children's Medical Center,
2-138-4 Mutsukawa, Minami-ku,
Yokohama 232-8555, Japan

T. Obata · M. Tomiyasu
Department of Biophysics, Molecular Imaging Center,
National Institute of Radiological Sciences,
Chiba, Japan

A. Errami
MRC-Holland,
Amsterdam, The Netherlands

K. M. Gibson
Department of Biological Sciences,
Michigan Technological University,
Houghton, MI, USA

G. S. Salomons · C. Jakobs
Metabolic Unit, Department of Clinical Chemistry,
VU University Medical Center,
Amsterdam, The Netherlands

H. Osaka
Molecular Pathology & Genetics Division,
Kanagawa Cancer Center Research Institute,
Yokohama, Japan

Published online: 06 January 2010